Solid Earth, 15, 405–436, 2024
https://doi.org/10.5194/se-15-405-2024

Solid Earth Open Access EGU

Lahar events in the last 2000 years from Vesuvius eruptions – Part 1: Distribution and impact on densely inhabited territory estimated from field data analysis

Mauro Antonio Di Vito[1], Ilaria Rucco[2], Sandro de Vita[1], Domenico Maria Doronzo[1], Marina Bisson[3], Mattia de' Michieli Vitturi[3], Mauro Rosi[4], Laura Sandri[5], Giovanni Zanchetta[4], Elena Zanella[6], and Antonio Costa[5]

[1]Istituto Nazionale di Geofisica e Vulcanologia – Sezione di Napoli Osservatorio Vesuviano, Naples, Italy
[2]School of Engineering and Physical Sciences, Heriot-Watt University, Edinburgh, UK
[3]Istituto Nazionale di Geofisica e Vulcanologia – Sezione di Pisa, Pisa, Italy
[4]Dipartimento di Scienze della Terra, Università di Pisa, Pisa, Italy
[5]Istituto Nazionale di Geofisica e Vulcanologia – Sezione di Bologna, Bologna, Italy
[6]Dipartimento di Scienze della Terra, Università di Torino, Turin, Italy

Correspondence: Mauro Antonio Di Vito (mauro.divito@ingv.it)

Received: 14 June 2023 – Discussion started: 1 August 2023
Revised: 3 January 2024 – Accepted: 26 January 2024 – Published: 3 April 2024

Abstract. Lahars represent some of the most dangerous phenomena in volcanic areas for their destructive power, causing dramatic changes in the landscape with no premonitory signs and impacting the population and infrastructure. In this regard, the Campanian Plain turns out to be very prone to the development of these phenomena, since the slopes of the Somma–Vesuvius and Campi Flegrei volcanoes, along with the Apennine reliefs, are mantled by pyroclastic deposits that can be easily remobilized, especially after intense and/or prolonged rainfall.

This study focuses on the analysis of pyroclastic fall and flow deposits and of the syn- and post-eruptive lahar deposits related to two sub-Plinian eruptions of Vesuvius in 472 CE (Pollena) and 1631. To begin with, historical and field data from the existing literature and from hundreds of outcrops were collected and organized into a database, which was integrated with several new pieces of data. In particular, stratigraphic, sedimentological (facies analysis and laboratory), and archeological analyses were carried out, in addition to rock magnetic investigations and impact parameter calculations. The new data are also referenced to the finding of ash beds in more distal areas, which were included in new isopach maps for the two sub-Plinian eruptions.

The results show that for both eruptions the distribution of the primary deposits is wider than previously known. A consequence of these results is that a wider areal impact should be expected in terms of civil protection, as the sub-Plinian scenario is the reference one for a future large eruption of Vesuvius. Such a distribution of the pyroclastic deposits directly affects the one of the lahar deposits, also because a significant remobilization took place during and after the studied eruptions, which involved distal phreatomagmatic ash. From these integrated analyses, it was possible to constrain the timing of the deposition and the kind of deposits remobilized (pyroclastic fall vs. flow), and it was possible to calculate the velocities and dynamic pressures of the lahars and ultimately infer the lahar transport and emplacement mechanisms.

The multidisciplinary approach adopted in this work shows how it is crucial to assess the impact of lahars in densely populated areas even at distances of several to tens of kilometers from active volcanoes. This especially applies to large parts of the densely populated areas around Somma–Vesuvius up to the nearby Apennine valleys.

Published by Copernicus Publications on behalf of the European Geosciences Union.

1 Introduction

The movement of volcaniclastic mass flows and the consequent damage along the flanks of active volcanoes and perivolcanic plains represent a constant threat to inhabited areas and populations (e.g., Waitt et al., 1983; Lowe et al., 1986; Pierson, 1985; Newhall and Punongbayan, 1996). Such systems are variably fluidized, gravity-driven flows that consist of a mixture of pyroclastic sediment and water. They can be triggered by various mechanisms, among which the most common are intense or prolonged atmospheric precipitation (Arguden and Rodolfo, 1990; Rodolfo and Arguden, 1991; Pareschi et al., 2000; Rodolfo, 2000; Scott et al., 2001; Vallance and Iverson, 2015). Such precipitation or water runoff, especially during and/or after the eruptions, can cause the remobilization of pyroclastic deposits evolving into water-saturated multiphase systems called lahars (e.g., White et al., 1997; Sheridan et al., 1999; Scott et al., 2001; Baumann et al., 2020). The last century was affected by a significant number of highly impacting lahar events associated with well-studied explosive volcanic eruptions worldwide, such as at Colima (Mexico) in 1913 (Rodriguez-Sedano et al., 2022), Nevado del Ruiz (Colombia) in 1985 (Voight, 1990), Ruapehu (New Zealand) in 2007 (Lube et al., 2012), and Merapi (Indonesia) in 2011 (Jenkins et al., 2015).

According to Rodolfo (2000), Sulpizio et al. (2006), and Vallance and Iverson (2015), volcaniclastic mass flows can be generated at variably long time intervals, spanning from eruptive to post-eruptive phases of tens to hundreds of years. In the case that these flows are directly related to volcanic eruptions and occur during or shortly after the eruptive event, lahars are defined as syn-eruptive and can represent an important multihazard factor in the short to middle term for perivolcanic areas (Rodolfo, 2000; Sulpizio et al., 2006). Instead, in that case that they are unrelated to any eruption dynamics and occur during long periods of volcanic quiescence, they are defined as post-eruptive (Vallance and Iverson, 2015) and can represent a long-term hazard factor (e.g., Siebe et al., 1999; Pareschi et al., 2002; Zanchetta et al., 2004a, b; Sulpizio et al., 2006). Usually, post-eruptive lahars are not accounted for in the assessment of volcanic hazard, although their study is important for hydrogeological hazard assessment and long-term territorial planning.

In this sense, from the hazard assessment point of view, one of the priorities concerns the assessment of areas potentially exposed to such a threat, taking into account the temporal recurrences of the phenomena (over days to months after an eruption or years to decades after) and physical features of the volcaniclastic mass flows (volume, thickness, velocity, dynamic pressure, concentration, and invasion areas). We stress the fact that the definition of syn-eruptive lahars (Sulpizio et al., 2006; Vallance and Iverson, 2015) adopted in the present work is important when accounting for the multihazard of explosive eruptions, which in areas like Vesuvius and surroundings should not be neglected for assessment and mapping purposes (de' Michieli Vitturi et al., 2024; Sandri et al., 2024). The methodology used in this work is geological (see Sect. 3.2), and the syn-eruptive definition of lahars is necessary to avoid underestimations of the volcanic hazard from sub-Plinian eruptions at Vesuvius.

A lot of the existing literature has analyzed the hazard related to volcaniclastic mass flows on the flanks of active volcanoes through the reconstruction of historical and prehistoric events (e.g., Scott, 1989; Scott et al., 1995; Vallance and Scott, 1997; Zaragoza et al., 2020) or by using empirical relationships or physical models (e.g., Macedonio and Pareschi, 1992; Costa, 1997; Iverson et al., 2000; Walsh et al., 2020). However, the areas affected by these phenomena can be extended well beyond the boundaries of the volcanic complex, also including the surrounding plains and the downwind-lying mountainous areas, which are subjected to tephra fallout sometimes even at great distances from the volcano (e.g., Siebe et al., 1999; Pareschi et al., 2000, 2002; Zanchetta et al., 2004a, b; Di Crescenzo and Santo, 2005). In these areas, volcaniclastic mass flows may harm victims and cause damage, even where considered safe or scarcely affected by other volcanic hazards.

In this paper, we present the results of a multidisciplinary study, including geomorphological, stratigraphic, sedimentological, and rock magnetic investigations, as well as impact parameter calculations by reverse engineering from the deposits. These investigations followed several surveying campaigns carried out in natural exposures, archeological excavations, and trenches dug specifically for this purpose in the plain surrounding the Vesuvius edifice and along the Apennine valleys (Fig. 1). One of the goals of this study is to show the presence of lahar deposits even in areas several kilometers from the source areas of the Apennine hills and Somma–Vesuvius edifice, demonstrating the high mobility of these flows. Indeed, these two areas acted as source areas because they were largely affected by deposition of primary pyroclastic deposits from Plinian and sub-Plinian Somma–Vesuvius eruptions. The study of past lahar deposits has been useful for understanding the feeding drainage basins, their extent and facies variations with distance from the source area, and the associated impact on the landscape. As already pointed out by Di Vito et al. (2013, 2019a, b), in the past 4.5 kyr repeated lahar and flooding episodes related to the main eruptions of Somma–Vesuvius and Campi Flegrei volcanoes have strongly struck the Campanian Plain and its human settlements, influencing their partial or total abandonment. In particular, for the areas around Vesuvius, these phenomena included (i) large-volume and high-energy lahars originating from the volcanic edifice, which affected the volcanic apron; (ii) large flooding phenomena, i.e., overflowing of water affecting the Campanian Plain; and (iii) lahars originating from the perivolcanic mountains that affected the Apennine valleys and invaded the areas of the plain at their mouths. All of these phenomena differ from each other in terms of the amount and grain size of the involved sediment. The data and

pieces of information described here were the basis for validating a new model for lahar transport (de' Michieli Vitturi et al., 2024), which was applied for assessing the related hazard at Vesuvius and Campanian Plain (Sandri et al., 2024).

The structure of the work consists of an integrated geological, geomorphological, stratigraphic, and sedimentological study, a paleomagnetic and sediment–mechanic impact assessment calculation, and a comprehensive discussion on the lahar problem in the Campanian Plain.

2 Geological setting

The study area is part of the Campanian Plain, which includes the lowlands surrounding Mount Vesuvius volcano and the nearby Apennine ridges and valleys (Fig. 1). The orography of the area is characterized by three WNW–ESE-trending mountain ridges that border the plain eastward, with an elevation ranging from 500 to 1600 m a.s.l. and slope angles from 30 to 60°. From north to south, the Avella–Partenio, Lauro–Visciano, and Sarno–Quindici mountain ridges are separated by two depressions: the Avella–Baiano Valley, in which the alluvial plain of the Clanio river occurs, and the Lauro valley. Both are narrow valleys that widen toward northwest, among the cities of Cicciano, Nola, and Palma Campania (Fig. 1). The reliefs are characterized by a high drainage density, associated with a poorly developed and torrential hydrographic network, which over time has favored the incision and dismantling of the pyroclastic cover on the ridges and the development of numerous detrital conoids that connect with the main valley floor (Di Vito et al., 1998).

Vesuvius, or more properly Mt. Somma–Vesuvius, is a composite central volcano less than 39 000 years old composed of the remnant of the oldest Mt. Somma edifice, dismantled by repeated episodes of caldera collapse, and the more recent Mt. Vesuvius grown inside it. Its volcanic history is characterized by an initial phase, dominated by low-energy effusive and explosive eruptions, which ended around 22 000 years ago. Since then, the volcano has generated four Plinian eruptions with VEI 5–6, each preceded by long periods of quiescence and all accompanied by a summit caldera collapse (Somma caldera; Cioni et al., 1999). The last Plinian eruption occurred in 79 CE and once again modified the Somma caldera, inside which the recent cone has subsequently grown due to an alternation of periods of an open conduit with persistent Strombolian and effusive activity, and long periods of quiescence with an obstructed conduit, interrupted by high-energy sub-Plinian eruptions. In historical times, the other more energetic events were the sub-Plinian "Pollena" (472 CE) and 1631 eruptions (Santacroce et al., 2008). The last eruption occurred in 1944 and caused the return to obstructed conduit conditions, which characterize the current quiescent phase of the volcano. The rock composition varies from slightly silica-undersaturated (K-basalt to K-trachyte) to highly silica-undersaturated (K-tephrite to K-phonolite). The Somma–Vesuvius complex is characterized by a well-developed radial drainage network, which feeds an extensive volcaniclastic apron that morphologically connects the edifice with the surrounding plain (Santacroce et al., 2003). It represents the active southern termination of the Plio-Quaternary volcanic chain that borders the eastern Tyrrhenian margin (Peccerillo, 2003). Volcanism in this margin is related to the extensional tectonic phases that accompanied the anticlockwise rotation of the Italian peninsula during the complex interaction between the Africa and Eurasian plates, which generated the Apennine thrust-and-fold belt (Ippolito et al., 1973; D'Argenio et al., 1973; Finetti and Morelli, 1974; Bartole, 1984; Piochi et al., 2004; Patacca and Scandone, 2007; Vitale and Ciarcia, 2018). The extension along the Tyrrhenian margin of the Apennine chain was accommodated by the activation of NW–SE normal faults and NE–SW normal to strike-slip transfer fault systems, which dismembered the chain in horst-and-graben structures and allowed magma to reach the surface and feed the volcanism (Mariani and Prato, 1988; Faccenna et al., 1994; Acocella and Funiciello, 2006). The Campanian Plain is one of these grabens that hosts the Neapolitan volcanic area. It is a NW–SE elongated structural depression, filled by a thick sequence of marine and continental sedimentary deposits and volcanic–volcaniclastic successions that compensated for its subsidence, leading to a complete emersion at around 39 ka (Brocchini et al., 2001; De Vivo et al., 2001; Santangelo et al., 2017). This graben is bordered toward NW, NE, and SE by the Meso-Cenozoic carbonate and terrigenous successions of the Apennine chain and is subdivided in minor NE–SW-oriented horst-and-graben structures (Carrara et al., 1973; Finetti and Morelli, 1974; Fedi and Rapolla, 1987; Brancaccio et al., 1991). Neapolitan volcanoes lie on these second-order structural highs (Marotta et al., 2022, and reference therein), and the products of their most powerful eruptions blanketed the Apennine reliefs and filled their valleys with several meter-thick covers of pyroclastic fall deposits, composed of pumice lapilli and ash layers separated by paleosols (Pareschi et al., 2002; Bisson et al., 2007; Cinque and Robustelli, 2009; Gurioli et al., 2010).

In terms of water drainage, the pyroclastic cover has peculiar geotechnical characteristics, such as a positive correlation between grain size and permeability, which enabled the development of lahars in the area. In particular, coarser pumice layers are characterized by inter-clast void spaces that control water accumulation, instead of ash layers, soils, and paleosols by a high water retention capacity (Andosol-like soils), so that the differential behavior can regulate equilibrium among deposit stability vs. remobilization (Fiorillo and Wilson, 2004).

Regarding the volcanic activity of Vesuvius in the last 2000 years, the largest eruptions after the 79 CE Plinian one were two sub-Plinian eruptions, the 472 CE Pollena and 1631 ones, but several other effusive and explosive events occurred in historical times. In the Campanian Plain, lahar de-

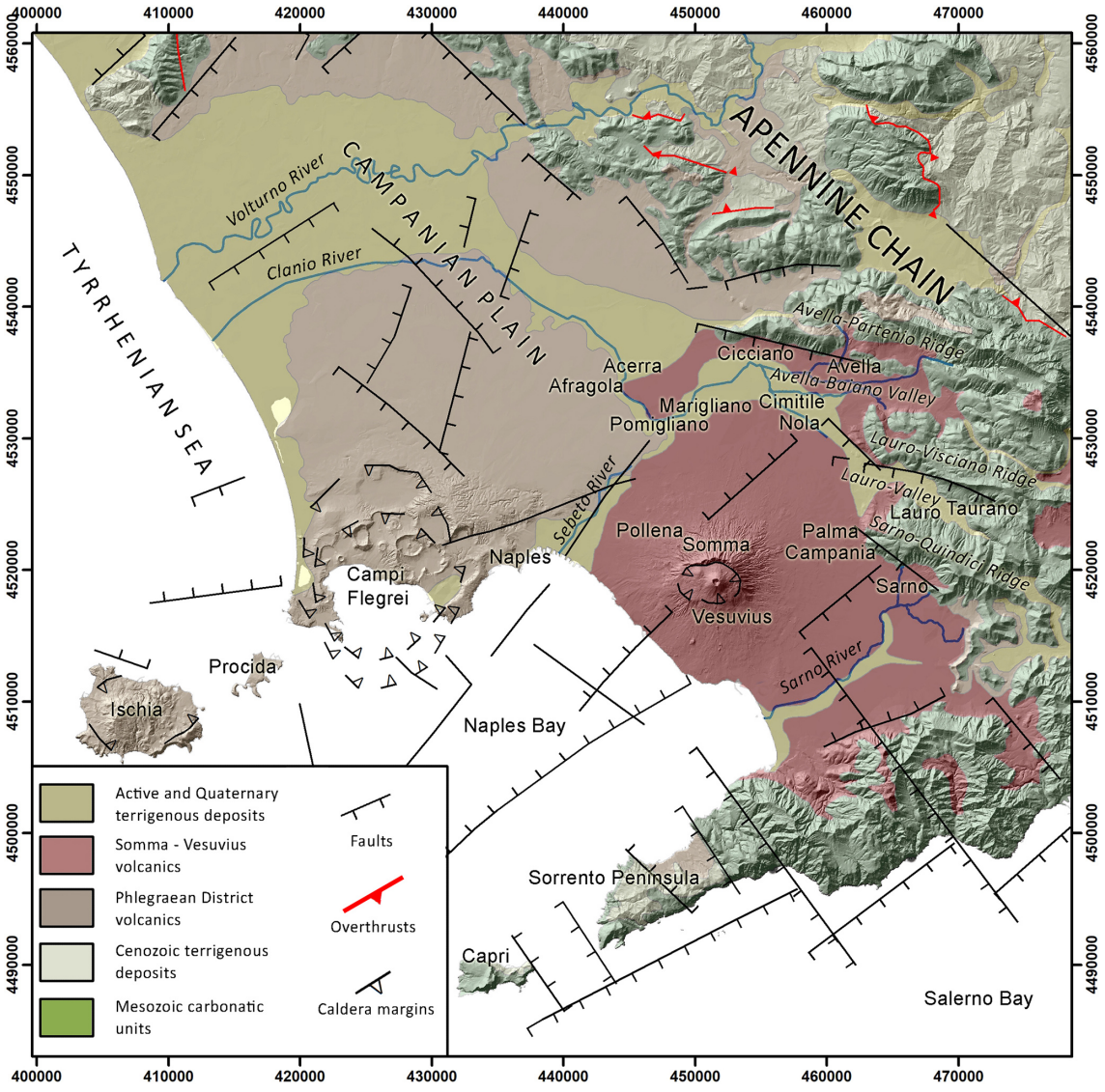

Figure 1. Geological and structural sketch of the Campania region on a shaded relief derived from the TINITALY DEM. The coordinates are expressed in WGS 84 UTM N33 (modified after Orsi et al., 1996).

posits related to these two eruptions are quite abundant due to past heavy rains (Fiorillo and Wilson, 2004; Zanchetta et al., 2004a; Stanzione et al., 2023). Also, the sub-Plinian scenario is of interest for civil protection purposes, which is why in the present work we focus on the 472 CE Pollena and 1631 eruptions. Particular attention is given to the distribution of the primary pyroclastic deposits and related syn-eruptive lahars, which are mass flow events directly related to specific eruptions, even if the condition is not necessarily that of an event contemporaneous to the eruption. Those deposits are mainly composed of $>90\,\%$ fragments from the parental eruption, while the remaining fragments pertain to other eruptions mixed by volcaniclastic colluvium (Sulpizio et al., 2006). The syn-eruptive feature is thus related to the remobilization of pyroclastic deposits more than to the exact timing of lahar emplacement, the latter being of the order of max a few years (before humification processes or significant human activities could occur). Such a feature distinction is important because it is directly related to volcanic hazard.

3 Materials and methods

3.1 Evidence from historical sources

We collected data from historical sources, maps, documents, and newspapers to supplement the geological data, gathered directly or indirectly, for the definition of the areal distribution of the syn-eruptive and post-eruptive lahar deposits at Vesuvius and in the surrounding region. Such collection con-

cerned the phenomena that took place starting from the sixteenth century CE to 2005. This time span has been chosen depending on data availability and to show the high recurrence of events over time in the area. The data were collected and grouped not only by years but also by the municipal areas existing at those times. It should be noted that the distribution of the data can be affected by the different urbanization over time and by the presence of damage to people, infrastructure, and goods, as well as economic activities and settlements. In the absence of local weather data series over the analyzed period, we assumed that the phenomena of remobilization of the pyroclastic deposits, and the consequent generation of large flooding events and volcaniclastic mass flows, coincided with extreme weather events often described and reported in the analyzed sources. We identified about 500 individual reports, covering events between the sixteenth century CE and 2005 that took place in 97 different municipalities. The data were organized in a geospatial database so that it was possible to define different areas affected by frequent syn-eruptive floods and lahars, concomitant with or related to the sub-Plinian eruption of 1631, to be used as a benchmark for the main geological analyses. We could not add the Pollena eruption to this historical data set, as there are no available sources for similar occurrences other than documents derived from archeological excavations (see next sections).

The municipalities with the highest number of reports are Sarno (43), Salerno (32), Siano (26), Vietri sul Mare (22), Bracigliano (21), Nocera Inferiore (20), Maiori (19), and Quindici (17) (Fig. 1). The number of events of greatest intensity, which affected more than five municipal territories at the same time, is 19. Some of these occurrences result closely connected with the volcanic events of Vesuvius, such as those that occurred in 1631, 1823, 1910, 1949, and 1954, simultaneously or within months to a few years after the Vesuvius eruptions of 1631, 1822, 1906, and 1944.

The absence of information in the Lauro and Avella–Baiano valleys is likely due to the absence of detailed descriptions of alluvial events or more likely to the position of the inhabited areas generally located on the hills and thus far from the lower part of the valleys. The investigated area was affected many times by post-eruptive lahar events due to the presence of thick, variably weathered pyroclastic deposits mantling the steep slopes of Somma–Vesuvius and the Apennines. One of the most recent events occurred on 5 May 1998, when 16 h of prolonged heavy rainfall triggered a huge number of Apennine slope failures toward the towns of Quindici, Bracigliano, Siano, Sarno, and San Felice a Cancello, all located near the Apennine ridges east-northeast of Somma–Vesuvius (Fig. 1). This catastrophic event involved an extension area of around 60 km^2 and a volume of more than 2×10^6 m^3 (40 % derived from materials eroded along the channels), harming 160 victims and causing severe damage to the mentioned towns (Di Vito et al., 2019a, and references therein).

3.2 Field and archeological investigations

We used a set of geological, stratigraphical, sedimentological, archeological, and pedological information for the reconstruction of the type of events, their emplacement mechanisms, timing, and impact on pre-existing structures and environment. Such an approach enabled us to cross-check geological and archeological evidence, allowing us to accurately fix the age of events. Conversely, the presence of well-dated primary pyroclastic deposits can define the age of human traces otherwise not easily datable. Furthermore, the identification of the "primary" deposit (fallout and pyroclastic current, along with the archeological findings) can give the absolute age (ante or post quem) of a given deposit. The definition of isochronic paleosurfaces can also contribute to the reconstruction of the paleo-environments affected by the deposition and of the variations that occurred during depositional processes. For this purpose, particular attention was paid to the basal contacts between the deposits. In some areas like Nola (10–15 km from Apennine source valleys), the lahar deposits directly overlie the primary pyroclastic deposits (for both the 472 CE Pollena and 1631 eruption), while in other areas some pyroclastic units or the whole primary deposits are missing (eroded) or lacking. Only correlation with the nearby areas permitted us to determine whether the emplacement of the lahars partly or significantly the eroded underlying primary deposits; in contrast, complete absence in the emplacement areas could also be due to the distribution of the latter. The analysis of the internal structure marked by sharp changes in grain sizes, color, presence of erosional unconformities, or interposition of lenses of coarser material also permitted the identification of one or more flow units within the same individual deposit package. The macroscopic characteristics of the sequences permitted some inferences on the transport and depositional mechanisms, while the grain-size and componentry analyses provided information on the source deposits that were remobilized. This brings us to another important definition, syn-eruptive vs. post-eruptive lahars, according to the definition of Sulpizio et al. (2006) and Iverson and Vallance (2015), which applies during or soon after the eruption vs. several years to centuries after the eruption ended, respectively. The macroscopic analysis allowed us to distinguish between the syn-eruptive and post-eruptive deposits. The first ones are defined by the occurrence of pyroclastic components with a lithology similar to the one of the primary deposits. The second ones are characterized by some evidence of depositional stasis like humified paleosurfaces below the lahar deposits and/or anthropogenic activities or by the presence of humified material and/or fragments of older eruptions in the deposits. All these characteristics allowed the correlation between the various volcaniclastic units for the whole set of studied sequences, marking the differences needed to hypothesize on the source and invasion areas.

We reviewed all the volcanological and archeological data collected during the last 20 years from drill cores, outcrops,

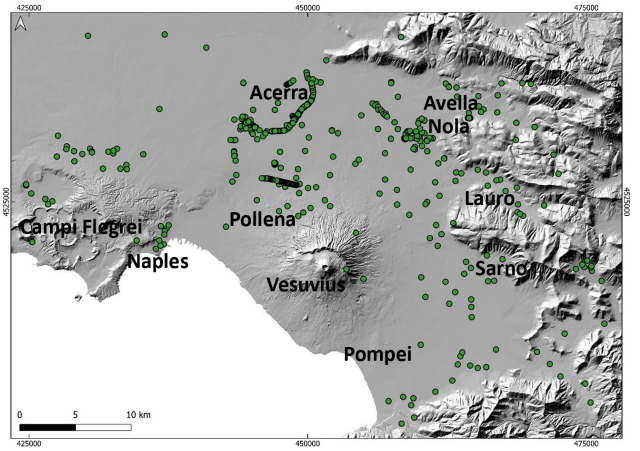

Figure 2. Shaded relief of the studied area and location of all the sites where stratigraphic analyses were carried out.

archeological excavations, and the existing literature in collaboration with colleagues from the Archeological Superintendence of the Campania region. The preliminary collection and analysis of the existing data permitted us to plan 100 new stratigraphic trenches (Fig. 2), with the aim of collecting stratigraphic, sedimentological, lithological, and chronological data on the primary pyroclastic and secondary (lahar) deposits. Particular attention was also paid to the geometric relations of these deposits to the paleotopography and preexisting anthropogenic structures.

The collected data were organized into a geospatial database (QGIS Platform), in which each point represents an investigated site linked to a series of information, such as the precise location, type of volcanic sequence, and stratigraphic features (primary and secondary units, thickness, type of deposit) (Di Vito et al., 2024). The data were visualized using a digital elevation model (DEM) of the Campanian Plain as reference topography and the UTM WGS 84 Zone 33N reference projection.

3.3 Geomorphological analysis

This analysis is aimed at identifying the macro-basins that fed the lahars in the study area after the two sub-Plinian eruptions (Pollena and 1631). The analysis was carried out on the basis of the slope distribution and the watersheds extracted from a digital elevation model (DEM). The DEM was derived from a lidar flight of 2012 (cell size of 10 m). In particular, six macro-basins characterized by slopes $> 20°$ were identified in the Somma–Vesuvius area, whereas 15 macro-basins with slopes $> 25°$ were identified in the Apennines to the east of the volcano (Fig. 3). The different slope thresholds are defined from previous studies (Pareschi et al., 2000, 2002; see also Bisson et al., 2013, 2014) and on the basis of a better analysis of the physical characteristics of the remobilized material, in turn related to the various types of deposits.

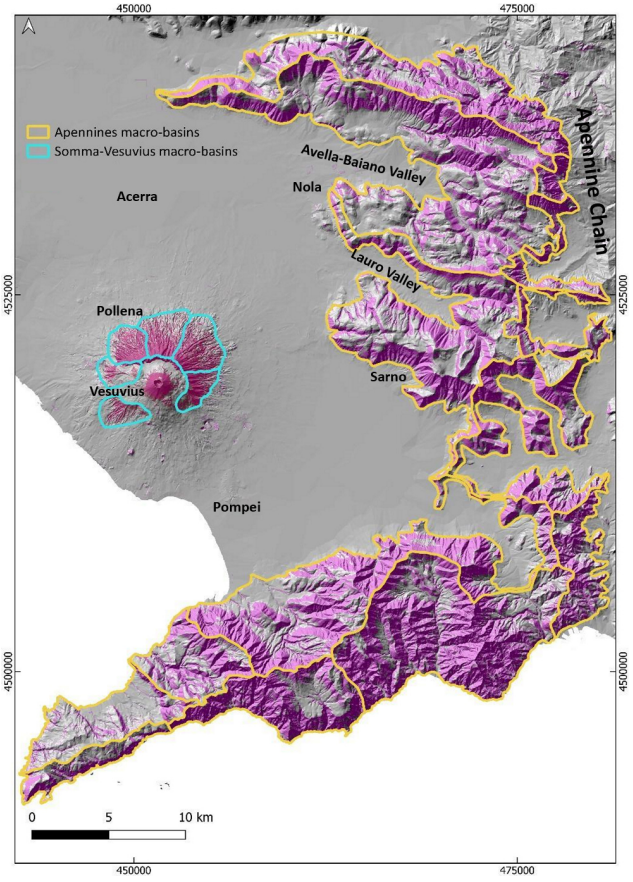

Figure 3. The macro-basins defined on the basis of their geomorphological features to study the areas of possible accumulation and mobilization of deposits, which are used in modeling lahar generation of future events.

In fact, on the steep slopes and in the valleys of Somma–Vesuvius the deposits are mainly ash-rich pyroclastic current deposits and subordinately lapilli fallout deposits, while on the Apennines they are ash and lapilli fallout deposits. Each basin was considered to be a single feeding unit for lahar generation, and this is an input for the modeling of possible future lahars in the companion papers (de' Michieli Vitturi et al., 2024; Sandri et al., 2024).

3.4 Laboratory and analytical work

3.4.1 Grain size

For selected study sites reported in Fig. 4, macroscopic analyses of the stratigraphic sequences were carried out in the field to first identify any homogeneities or similarities between the juvenile fraction of the primary and secondary deposits and then recognize the various volcaniclastic units. This was followed by sampling the deposits and carrying out laboratory analyses.

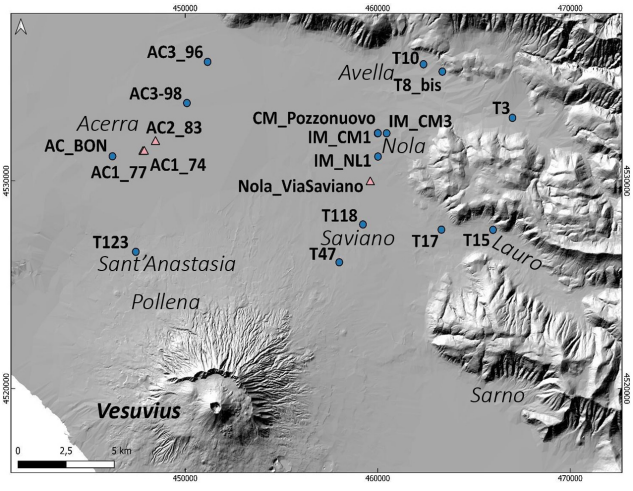

Figure 4. Location of sites at which the sampling was carried out for sedimentological and paleomagnetic analyses. The pink triangles represent the sites for which a paleomagnetic study was carried out (AC1_74, AC1_77, AC2_83, and Nola_Via Saviano). At several sites, multiple samples were taken at different stratigraphic heights; samples labeled with US were taken at CM_Pozzonuovo site (see the Results section).

In particular, the sampling was mostly made on the syn-eruptive lahar deposits, but also on the post-eruptive and, in a few cases, on the primary pyroclastic deposits. All lab analyses were performed in the laboratories of sedimentology and optical microscopy at the Istituto Nazionale di Geofisica e Vulcanologia, Sezione di Napoli Osservatorio Vesuviano (INGV–OV). The material samples were pre-heated at a temperature of 60–70 °C to eliminate any fraction of humidity and then quartered and sieved. To avoid any breaking of fragile clasts like pumices, the dry-sieving of the grain-size classes between −4 (a coarse limit variable depending on the sample) and 0 phi was made manually, while for the classes between 0.5 and 5 phi a mechanical sieving apparatus was used.

In particular, the fine-ash-rich deposit samples with a high degree of cohesion (with a significant amount > 0 phi) were diluted in distilled water, then boiled to remove all ash aggregates, before being analyzed for grain sizes following a wet procedure, and finally dried and weighed by class. The cumulative class > 5 phi was further separated by interpolation modeling (de' Michieli Vitturi et al., 2024). In the post-processing of the data, the GRADISTAT excel package by Blott and Pye (2001) was used to determine the main statistical parameters. On selected samples, a microscopic componentry analysis was performed, consisting of recognizing and separating the various lithotypes that compose the volcaniclastic deposits, which are juvenile, lithic, and crystal clasts. The clast recognition was made manually for the coarser fractions, while for the finest fractions it was necessary to use a reflected-light binocular microscope.

3.4.2 Input for impact parameters

A significant number of large clasts and boulders was also found embedded in the lahar deposits at different locations. These clasts have dimensions from several centimeters to several tens of centimeters in diameter, and their nature is variable: limestone, ceramic, brick, tephra, lava, sandstone, iron (in order of abundance). Most of the clasts are fragments of artifacts from buildings, structures, and other archeological finds of the Roman period, and their shape can be approximated in the field as ellipsoid. All these features suggest that they were entrained from substrate into the lahars to ultimately be deposited together with the main finer solid load of the lahars. In the dynamics of volcaniclastic mass flows like lahars and pyroclastic currents, the occurrence of boulder entrainment by flow dynamic pressure is recognized as a quite common feature (e.g., Zanchetta et al., 2004b; Pittari et al., 2007; Duller et al., 2008; Toyos et al., 2008; Cas et al., 2011; Carling, 2013; Doronzo, 2013; Jenkins et al., 2015; Roche, 2015; Martí et al., 2019; Guzman et al., 2020). The capability of a flow to entrain a clast is a function of flow properties (velocity, density), clast properties (dimension, density, shape), and dynamic pressure well syntheses and also quantifies such capability in terms of flow hazard (Toyos et al., 2008; Zuccaro and De Gregorio, 2013; Jenkins et al., 2015). In Appendix A, a theoretical scheme is presented to invert these field features for calculation of the impact parameters at a local scale.

3.4.3 Rock magnetism

The lahar deposits related to the Pollena eruption were analyzed by rock magnetism in the municipalities of Acerra (12 km from Somma–Vesuvius) and Nola (10–15 km from 10–15 km from Apennine source valleys) at four localities (Fig. 4), where the lahars interacted with anthropogenic structures. At each locality, we collected oriented samples, then measured about 200 specimens. We sampled both the deposit matrix and some potsherds embedded along three trenches (74, 77, and 83) and in the "Nola–Via Saviano" excavation. The purpose of the magnetic measurements was threefold. The first aspect was (i) evaluating the magnetic fabric of the deposits to infer the local to regional flow directions of the lahars and possibly their origin, whether from the Apennines or Vesuvius. The magnetic fabric in this type of deposit records the main flow direction (local or regional) followed during the emplacement processes. The second aspect was (ii) estimating the deposition temperature (T_{dep}) of the deposits to understand whether the lahar was triggered soon after the eruption or at later times. The hypothesis is that the temperature is higher in the case of syn-eruptive lahars deriving from hot (pyroclastic current) deposits and lower in all other cases. The third aspect was (iii) testing the relative sequence (contemporaneity) of the lahar emplacement with respect to the Pollena eruption. All hand samples were

oriented in situ with magnetic and solar compasses and reduced to standard sizes at the CIMaN-ALP laboratory (Peveragno, Italy), where all the magnetic measurements were made. In Appendix B, the adopted paleomagnetic techniques and nomenclature are described.

4 Results

4.1 Field stratigraphy and sedimentological features

In this study, data from about 500 sites were collected, covering an area of $> 1000\,km^2$ from the plain around the volcanic edifice to the Apennine valleys to the north and east (Fig. 2).

4.1.1 Pyroclastic deposits: Pollena and 1631 eruptions

The integration of the collected data with the existing ones (Rosi and Santacroce, 1983; Rosi et al., 1993; Rolandi et al., 2004; Sulpizio et al., 2005; Perrotta et al., 2006; Bisson et al., 2007; Santacroce et al., 2008; Gurioli et al., 2010; De Simone et al., 2011) allowed the reconstruction of the distribution maps for both the fallout and pyroclastic current deposits. In particular, the spatial distribution highlights that for both the Pollena and 1631 primary deposits, thick fine ash deposits are widely distributed and cover the coarse fallout sequence or the ground directly, modifying the isopachs reconstructed by previous authors (Sulpizio et al., 2006, and references therein; Figs. 5 and 6). This enlargement of the area affected can have important implications for the hazard evaluation in terms of possible damage to densely inhabited territory.

The area covered by the comprehensive isopach maps (including both lapilli and ash fallout) turns out to be wider than previously known, above all because we took into account the ash fallout that occurred during the final phreatomagmatic stages of the eruptions (Rosi and Santacroce, 1983; Sulpizio et al., 2005). The great availability and distribution of these ash deposits could explain the wide generation and distribution of the syn-eruptive lahars in the area. This has important implications for the evaluation of the source area and material available for the lahars accompanying and following these eruptions. Interestingly, there is an increase in the areas covered by pyroclastic deposits. The QGIS recalculated 10 cm isopach area covered by the fallout deposits is $837\,km^2$ (Pollena eruption) and $528\,km^2$ (1631 eruption), which compared to the lower values of $569\,km^2$ (Pollena eruption) and $158\,km^2$ (1631 eruption) after Sulpizio et al. (2006) give an extra surface of about 47 % and 230 %, respectively. Geotechnically, another implication is that the wide presence of fine and cohesive ash, not only on top of the coarse fallout sequences but also on the ground, prevented water infiltration, favoring surficial runoff and creating sliding surfaces (Baumann et al., 2020).

The area affected by accumulation of the 1631 eruption tephra-fallout deposits is wider than previously known, particularly toward the north, which follows the inclusion of the final ash deposits in the new isopachs. Interestingly, such

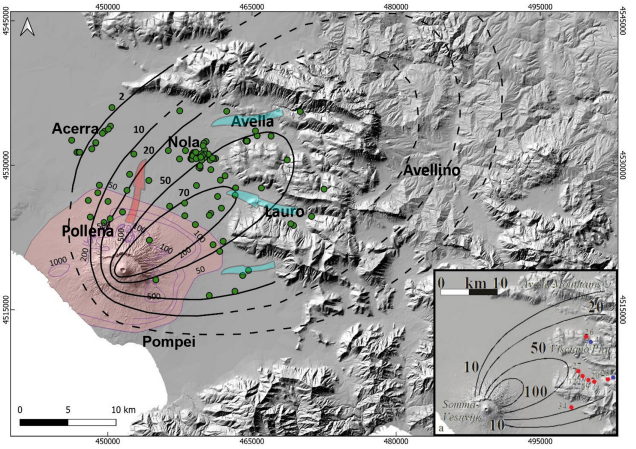

Figure 5. Pollena eruption: the black lines represent the isopachs (in cm) of the fallout deposits modified after Sulpizio et al. (2006) (in the inset) on the basis of the new collected data (green dots), while colored in pink is the area affected by the pyroclastic current deposits (isopachs in cm, purple lines) modified after Gurioli et al. (2010). The dotted isopachs are extrapolated. The light blue arrows represent the general remobilization of the pyroclastic fallout deposits and lahar propagation from the Apennine slopes, while the pink one represents the combined remobilization of the pyroclastic current and fallout deposits as well as lahar propagation from Somma–Vesuvius.

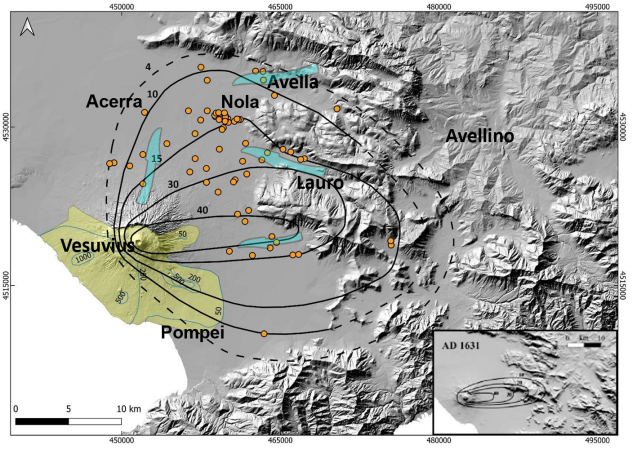

Figure 6. 1631 eruption: the black lines represent the isopachs (in cm) of the fallout deposits modified after Santacroce et al. (2008) (in the inset) on the basis of the new collected data (orange dots), while colored in yellow is the area affected by pyroclastic current deposits (isopachs in cm, light blue lines). The light blue lines represent the inferred distribution on the basis of an integration between field data and chronicles modified after Gurioli et al. (2010). The dotted isopachs are extrapolated. The light blue arrows represent the general remobilization of the pyroclastic fallout deposits and lahar propagation from the Apennine slopes and Somma–Vesuvius.

widening of the area agrees with the occurrence of lahars in the plain north of Vesuvius, as documented in historical sources (Rolandi et al., 1993; Rosi et al., 1993, and references therein) and as follows.

4.1.2 Lahar deposits

The lithological and sedimentological analyses carried out in the field allowed the macroscopic definition of the primary pyroclastic deposits affected by the remobilization and of the lahar deposits. In many cases, the archeological findings permitted us to define the local paleoenvironment and related land use, then permitted us to constrain the age and timing of the deposition.

We grouped all deposit descriptions into representative lithofacies to more directly characterize both the primary pyroclastic and lahar deposits (Table 2 and Fig. 7). Given the amount of data and description of the studied areas, we used these lithofacies to characterize a number of macro-areas between the Somma–Vesuvius sector and the nearby Apennine valleys (Appendix C).

Usually, the syn-eruptive lahar deposits directly overlie the primary pyroclastic deposits, sometimes eroding them. They have a matrix-supported texture, are composed of fine to very fine cohesive ash, and contain more or less abundant centimeter-sized pumice and lithic fragments. In general, these deposits consist of multiple depositional flow units, each one resulting from single-pulse "en masse" emplacement, the piling of which results from rapid progressive aggradation through multiple flow pulses, in analogy to dense pyroclastic currents (Sulpizio et al., 2006; Doronzo, 2012; Roche, 2012, 2015; Breard and Lube, 2017; Smith et al., 2018; Guzman et al., 2020; see Sulpizio et al., 2014, p. 56). Consequently, the studied lahars were modeled using a shallow layer approach (de' Michieli Vitturi et al., 2024). The different depositional flow units in the same deposit are distinguishable (still in continuity) from each other based on vertical granulometric changes, sparse pumice alignments, deposit layering, and/or unconformities. For example, compared to channelized pyroclastic currents, dense water flows, and floods, such depositional units (layers) could have been repeatedly emplaced, from bottom to top, under accumulation rates of a few tens to hundreds of $\mathrm{kg\,m^{-2}\,s^{-1}}$ (Lowe, 1988; Russell and Knudsen, 1999; Whipple et al., 2000; Girolami et al., 2010; Roche, 2015; Marti et al., 2019; Guzman et al., 2020). In various areas, such rapid sequential emplacement is suggested by the presence of water escape structures through the whole deposit by crossing the sequence of several units. These are vertical structures consisting of small "pipes" filled with fine mud transported by the escaping water and formed soon after the emplacement of the lahar units. The textural characteristics are variable even within the same site, but in general the deposits are massive and contain vesicles, from circular to flattened, coated by fine ash that adhered to the voids after water loss. For the syn-eruptive lahar deposits, the pumice fragments are those of the primary deposits. On the other hand, in the upper parts of the sequences it is not uncommon to find units that contain pumice fragments related to previous eruptions (9.0 ka BP "Mercato" and 3.9 ka BP "Avellino" Plinian eruptions), recognizable based on pumice texture and crystal content (Santacroce et al., 2008). In this second case, the lahar deposits are considered to be post-eruptive, meaning that the pyroclastic deposits older than the two studied sub-Plinian eruptions were progressively involved in advanced erosion of the

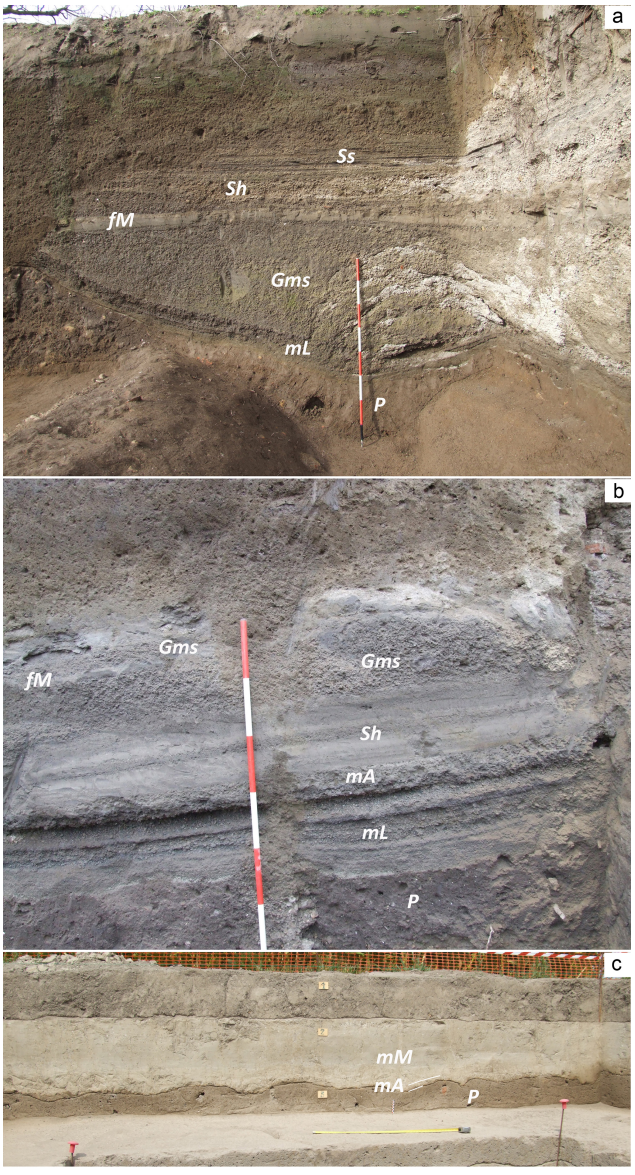

Figure 7. In these three photos of archeological excavations (**a–b** Nola at 10–15 km from Apennine source valleys; **c** Acerra at 12 km from Somma–Vesuvius), the main lithofacies recognized in the field are shown, including paleosols, pyroclastic deposits, and lahar deposits; the corresponding lithofacies descriptions are reported in Table 2.

Table 1. Symbol and description of the recognized lithofacies as well as photos representative of each of them.

Symbol	Lithofacies
P	Paleosol and humified surface, massive and composed of fine sand and silt from brown to dark brown, with several percentages of clay and organic matter. It indicates a stasis in the depositional processes.
mL	Alternation of massive lapilli layers. Pyroclastic fall deposit composed of pumice and scoria lapilli with sparse accidental lithics.
mA	Massive ash. Pyroclastic fall deposit composed of fine to coarse ash with sparse pumice fragments, scoriae and accidental lithics.
Gms	Massive gravel and sand deposit, matrix-supported and poorly sorted. The matrix is composed of fine to coarse sand, while the gravel clasts comprise scoria and pumice clasts from the pyroclastic fall deposits. The massive feature of the single layers suggests a rapid emplacement from a highly concentrated lahar.
mM	Massive mud deposit composed of fine sand, silt and clay, sometimes with sparse pumice and lithic clasts. It is generated from a mud-dominated lahar.
Sh	Horizontal lamination and bedding features in sands. The deposit is composed of an alternation of fine to coarse sand and gravel, which can be gradual or sharp. It comes from a hyper-concentrated lahar (less dense than the Gms one).
Ss	Scour and fill structures composed of fine to coarse sand, generally with a normal grading. A single structure consists of an erosive, concave upwards basal surface and a planar/convex top.
fM	Fine mud deposit composed of fine sand, silt and clay. It is generated when the lahar loses its energy and the fine grains settle gently.

slopes and valleys. The presence of slightly humified surfaces below the lahar deposits or traces of human artifacts, such as excavations and plowing, are considered to be evidence of a long period without deposition; also in this case, the lahars are considered to be post-eruptive. In other words, the similar componentry of the lahar and pyroclastic deposits and the evidence of short-term exposure between these two are strong indicators of the syn-eruptive occurrence of the lahar events. Instead, the absence of such features is more indicative of a post-eruptive origin, i.e., lahar events more spaced in time from the corresponding eruption.

In Appendix C, a description is reported for some of the most representative sequences, which were sampled in different areas throughout the plain (Figs. 2 and 4).

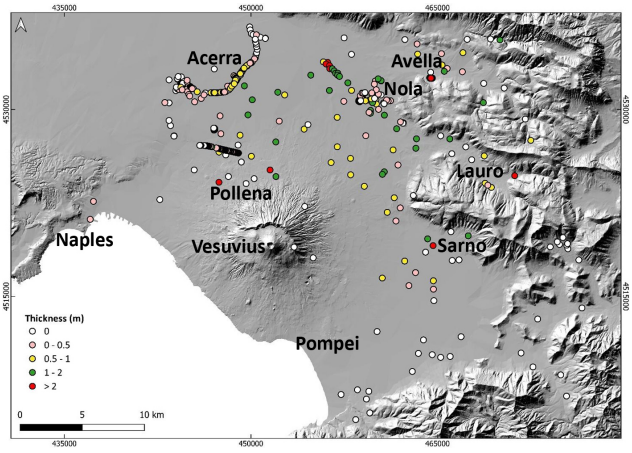

Figure 8. Distribution of the syn-eruptive lahar deposits related to the Pollena eruption. The 0 m points represent the studied sites where the lahar deposits were absent, and in some cases even the primary pyroclastic deposits below were absent; they are reported anyway, as their absence might not necessarily have occurred by no deposition (local erosion).

4.1.3 Distribution maps of the lahar deposits

Here we present distribution maps for the lahar deposits of the Pollena and 1631 eruptions (Figs. 8–11). The maps show the distribution of all thicknesses detected at the studied sites. In particular, the syn-eruptive Pollena lahar deposits are distributed in the NW quadrants of the volcano and in the Avella, Lauro, and Sarno valleys (see Fig. 1), with a thickness exceeding 1 m in the Vesuvius apron and in the plain between Nola and Cimitile at about 10–15 km from Apennine source valleys (see Figs. 1 and 8). A volume estimation of the remobilized deposits is of the order of 7×10^7 m^3 for the northern Vesuvius area and 4×10^7 m^3 for the Lauro Valley. Such volumes refer to the depositional areas and not to the detachment ones; for the latter see de' Michieli Vitturi et al. (2024) and Sandri et al. (2024). The provenance of the material at each site was inferred by sedimentological recognition and magnetic reconstruction. Then, the covered areas were subdivided into polygons in the geospatial database in order to weigh the local deposit thicknesses and estimate the volumes with a lower approximation.

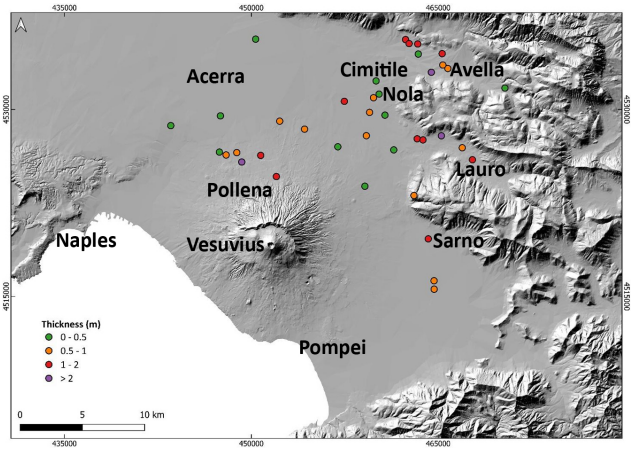

Figure 9. Distribution of the post-eruptive lahar deposits related to the Pollena eruption.

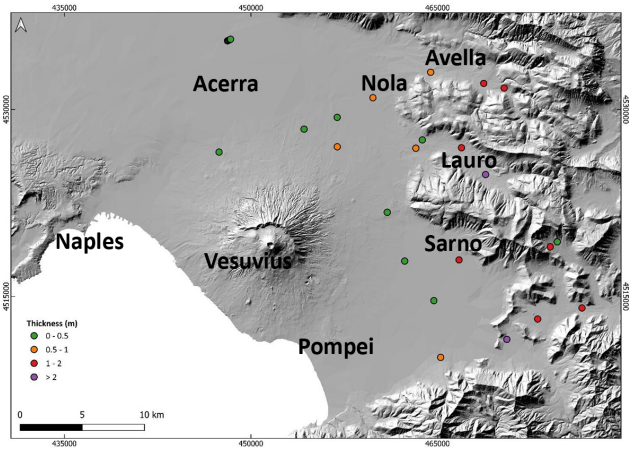

Figure 11. Distribution of the post-eruptive lahar deposits related to the 1631 eruption.

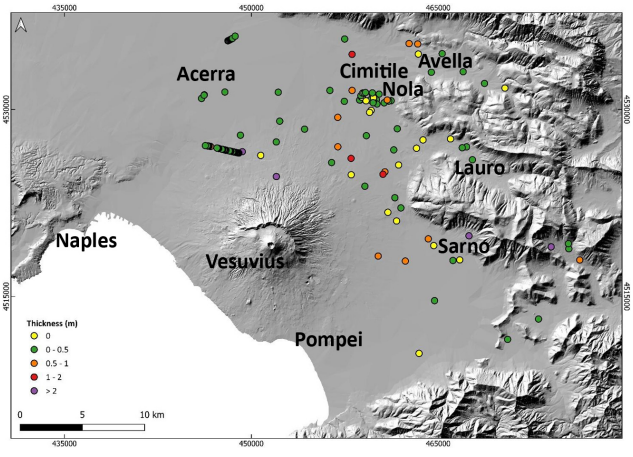

Figure 10. Distribution of the syn-eruptive lahar deposits related to the 1631 eruption. The 0 m points represent the studied sites where the lahar deposits were absent, and in some cases even the primary pyroclastic deposits below were absent; they are reported anyway, as their absence might not necessarily have occurred by no deposition (local erosion).

The post-eruptive lahar deposits of the Pollena eruption are more distributed in the Avella and Lauro valleys and in the plain north of the volcano close to the apron area (low-angle edifice outer slopes) (Figs. 1 and 9). Their deposits contain fragments from both the Pollena eruption and from preceding eruptions, suggesting that pyroclastic deposits of the older sequences were progressively eroded and involved in remobilization processes over time. As an example, in Fig. C1 it is to be noted that whitish pumice fragments from the Pomici di Avellino and Mercato eruptions were identified on top of the Pollena lahar deposits.

The distribution of the syn- and post-eruptive Pollena lahar deposits is related to the primary pyroclast deposition: the dense distribution of the lahar deposits north of Somma–Vesuvius depends on the presence of thick pyroclastic current deposits that were remobilized from the northern slopes of the volcano, while the distribution in the Apennine valleys is related to the fallout deposits that are thicker along the major Pollena dispersal axis (Fig. 5).

Above the Pollena pyroclastic and lahar deposits (both syn- and post-eruptive), the studied sequences at almost all the sites show the presence of a well-developed soil bed with many traces of cultivation, as well as of inhabited areas and buildings (Figs. C1–4). These traces and the presence of the soil bed are evidence of a progressive geomorphological stabilization of the territory. The occurrence of the 1631 sub-Plinian event determined a new phase of marked geomorphological instability for a large territory surrounding the volcano. In Fig. 10, the distribution of the syn-eruptive lahar deposits for the 1631 eruption in all the studied areas is shown, having a variable thickness of generally < 50 cm. Such a distribution mostly affected the areas of Acerra–Nola, Sarno, the Vesuvius apron, and the Apennine valleys (Figs. 1 and 10). Rosi et al. (1993) and Sulpizio et al. (2006) reported that floods and lahars heavily impacted (also with injuries and victims) the N and NE quadrants of Somma–Vesuvius soon after the eruption with a timescale of days (Rosi et al., 1993; see also the historical chronicles of Braccini, 1632), corroborating the syn-eruptive behavior of such lahars. Some lahar deposits are intercalated within the primary pyroclastic deposits, but in general they directly stand on top of the pyroclastic deposits (Rosi et al., 1993); both cases unequivocally constrain the syn-eruptive behavior of the 1631 eruption lahars.

In Fig. 11, minor post-eruptive lahar deposits of the 1631 eruption are reported, with a preferential distribution to the E quadrants of the volcano from N to S both on the plain and in the valleys. These deposits are still significant, with a thickness of around half a meter to a meter or more at a few points.

The distribution of the syn- and post-eruptive 1631 lahar deposits mainly reflects the major dispersal axis affecting the fallout deposit distribution, while the pyroclastic current deposits were minorly remobilized as exposed on the gentler slopes of southwestern Vesuvius (Fig. 6).

4.1.4 Sedimentological characteristics of the Pollena lahar deposits

The field analysis was carried out at about 500 different sites for the construction of the database and maps, while the laboratory analysis was carried out on 30 samples representative of the different areas. The results of the grain-size analyses (cumulative curves and statistical parameters) are presented in Fig. 12 and Table 1.

Petrological analysis of the syn-eruptive lahar deposits has not been performed because the lithology (color, texture, mineral content) of the components is the same as the juvenile material of the primary deposits described in Sulpizio et al. (2005). The loose crystals consist of sanidine, leucite, biotite, and pyroxene fragments. Based on the results of the grain-size analyses, the coarser classes are defined from -4 to -1 phi, the medium ones from -0.5 to 2.5 phi, and the finest one from 3 phi. The juvenile pumice clasts are a ubiquitous component of the lahar deposits (both syn- and post-eruptive), but they decrease with distance for the finer grain-size classes, while the crystal content increases with the same progression. The lithic clasts are abundant for the coarser classes; they decrease with distance for the medium classes and increase again for the finer classes.

Field observations and grain-size analyses highlight significant differences between the sectors of Lauro Valley, Avella–Baiano Valley, and Somma–Vesuvius. A common feature among the three sectors is that the lahar deposit samples are mostly massive, poorly sorted and polymodal; only a few samples are moderately sorted, and unimodal (sorting < 1.5 phi). On the other hand, the grain-size modes found show some interesting differences (in Fig. 12 the cumulative curves are shown). The coarse modes for Lauro Valley and Avella–Baiano Valley span from fine and medium lapilli to coarse ash, while for Somma–Vesuvius they span from coarse to fine ash. The medium modes for Lauro Valley and Avella–Baiano Valley span from coarse to medium ash, while for Somma–Vesuvius they span from medium to fine ash. The fine modes for Lauro Valley, Avella–Baiano Valley, and Somma–Vesuvius span from medium to fine ash. All these differences basically depend on the origin of the primary pyroclastic deposits (fallout vs. pyroclastic currents), which were remobilized from different sectors: the Apennines and Somma–Vesuvius. The grain-size analysis is used as input information for the lahar transport model (de' Michieli Vitturi et al., 2024) aimed at assessing the related hazard (Sandri et al., 2024).

4.2 Magnetic results

Both Acerra (12 km from Somma–Vesuvius) and Nola (10–15 km from Apennine source valleys) localities show a well-defined magnetic fabric for the Pollena syn-eruptive lahar deposits. Principal susceptibility axes ($K_1 \geq K_2 \geq K_3$) are clustered. Magnetic lineation (K_1) and magnetic foliation (K_3, pole of the plane) are mostly sub-horizontal or gently imbricated. The anisotropy degree P (K_1/K_3) is mostly lower than 1.060 but can reach high values like 1.200. At Acerra, the magnetic foliation is always dominant, and the fabric is oblate. The P_j is linearly correlated with the mean susceptibility (k_m). In Appendix B, the full nomenclature is defined for completeness. The magnetic fabric has a horizontal magnetic foliation and a clustered magnetic lineation, whose mean direction is NE–SW. Considering the chaotic nature of the lahar deposits, the high P_j and the clustered susceptibility axes can highlight a channelized flow (Fig. 13). At Nola, instead, the fabric is both prolate and oblate, and P_j is lower than 1.040. The susceptibility axes are more dispersed than at Acerra, but mean magnetic lineation clearly shows a NW–SE direction. If one considers the oblate specimens only, the magnetic foliation is sub-horizontal; on the contrary, the magnetic foliation of the prolate specimens is steeply dipping (65°) toward SE. At Nola, the flow direction inferred by AMS is consistent and parallel to the invasion basin.

At Acerra, the T_{dep} interval is 120–140 °C, while for Nola T_{dep} is lower than 120 °C (Fig. 14). In the Nola case, a low-temperature magnetization component lower than 120 °C cannot be directly considered to be a thermal remanent magnetization (TRM). In fact, the low-T_b Earth field component of magnetization can also be produced by a viscous remanent magnetization (VRM), acquired during exposure to weak fields (Bardot and McClelland, 2000). The acquisition of the VRM depends on the duration of the exposure. For an age around that of the Pollena eruption, the minimum T_{dep} which can be distinguished is ca. 120 °C. For this reason, we considered the Nola lahar to be emplaced at low temperature.

The mean paleomagnetic direction for each locality, calculated using Fisher's statistics, is well-defined, and its directional value and confidence limits do not overlap (Fig. 15). Thus, the two directions are statistically distinguishable at 95 % confidence limits. Since a paleomagnetic direction is a record of the Earth's magnetic field acting during the emplacement, it follows that the lahar deposits at the two localities are not synchronous.

Overall, all magnetic measurements just discussed show distinctly different characteristics between Acerra and Nola, clearly indicating two distinct events of emplacement.

4.3 Lahar dynamics

By inverting the field evidence and data, it is possible to reconstruct the macroscopic flow dynamics that occurred in the

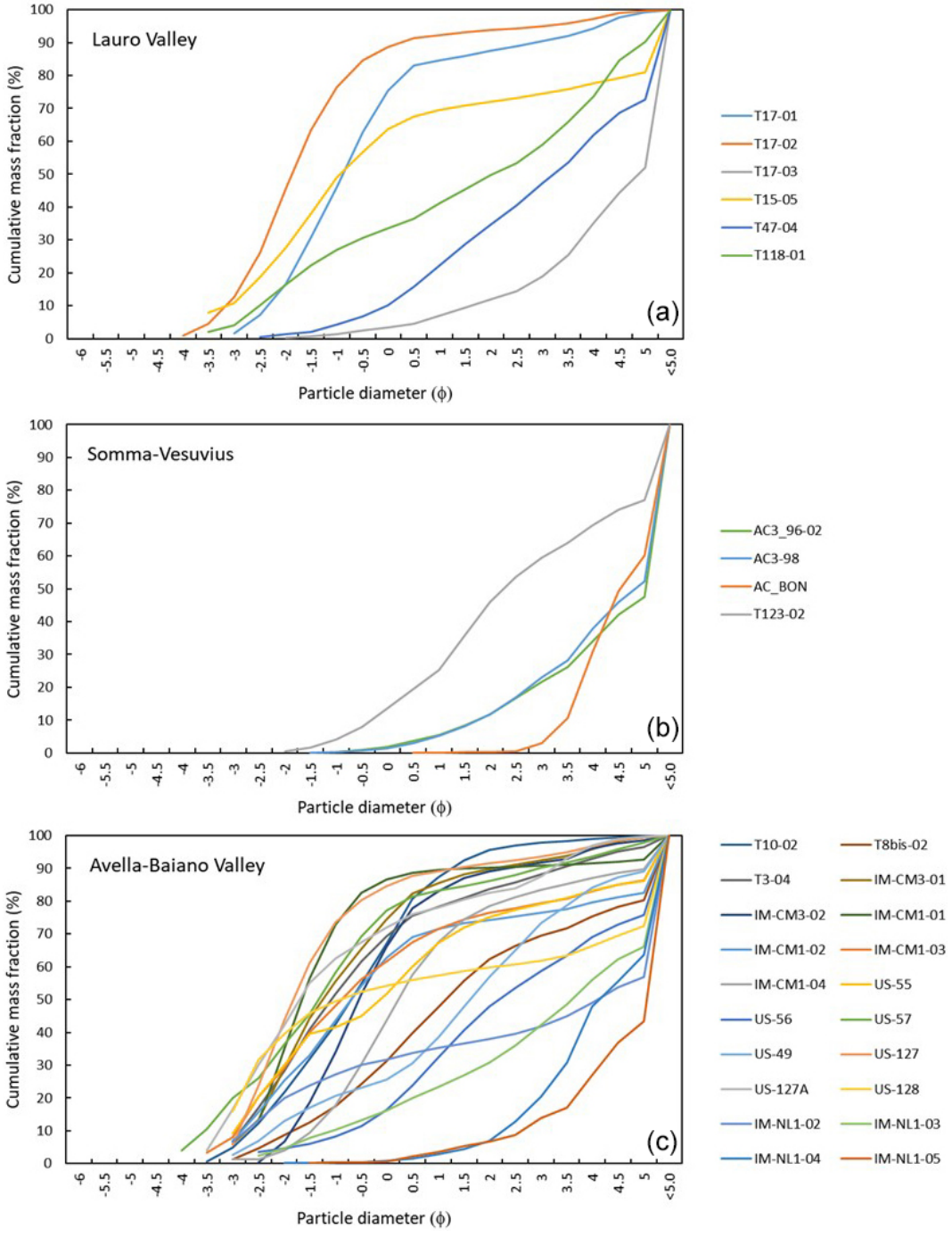

Figure 12. Cumulative curves of the grain-size analysis of the samples taken at the locations reported in Fig. 4 and subdivided into three sectors: Lauro Valley **(a)**, Somma–Vesuvius **(b)**, and Avella–Baiano Valley **(c)**.

lahar invasion, which are particularly interesting to understand the impact that those lahars had on the Vesuvius territory. As already described, the lahar deposits show thicknesses that are variable from several centimeters to a few meters, and this can depend on multiple local factors: (i) topography, (ii) distance from the source, (iii) erosion, and (iv) source area and type of remobilized sediment (variably sized fallout vs. flow deposits). In particular, thicker deposits are found near the mouth of the valleys and in the flat alluvial plain, as shown in the deposit distribution maps. On the other hand, the deposits show a generally tabular-like shape (Fig. 7), with an average thickness of the order of 0.5–1 m for several studied sites, which is the first evidence of the lahar impact and mass flow emplacement in the area. In

Table 2. Historical archive of lahar and alluvial events related to the four most significant Vesuvius eruption in the last 4 centuries and the municipalities affected by such events.

Eruption	Lahar/intense alluvial event	Municipalities affected
December 1631	16/12/1631	Sant'Anastasia, San Giorgio a Cremano, Massa di Somma, Somma, Ottaviano, San Sebastiano, Trocchia, Torre del Greco, Portici, Pugliano, Madonna dell'Arco, Palma, Nola Arpaia, Arienzo, Cicciano, Marigliano, Benevento, Avellino
October 1822	24/01/1823	Amalfi, Bracigliano, Cava de' Tirreni, Cetara, Minori, Nocera Inferiore, Pagani, Salerno, Sant'Egidio del Monte Albino, Tramonti, Vietri sul Mare
	12/02/1823	Maiori
	12/04/1823	Sarno
	18/10/1823	Corbara, Praiano, Sant'Egidio del Monte Albino, Sarno, Siano
	15/11/1823	Salerno
April 1906	24/10/1910	Amalfi, Boscotrecase, Cercola, Cetara, Ercolano, Giffoni Valle Piana, Maiori, Marano di Napoli, Minori, Napoli, Pollena Trocchia, Torre del Greco, Vico Equense, Vietri sul Mare, Sant'Anastasia, San Giorgio a Cremano, Sarno, Scala, Pomigliano d'Arco, Portici, Ravello, Salerno
March 1944	02/10/1949	Lauro, Maiori, Minori Nocera Inferiore, Sarno, Vietri sul Mare
	25/10/1954	Cava de' Tirreni, Maiori, Minori, Nocera Inferiore, Salerno, Tramonti, Vietri sul Mare

terms of runout distance, the lahars traveled for 10 to 15 km from sources (Somma–Vesuvius and Apennine detachment areas) based on the geospatial database that includes all studied sites. It was possible to infer the source areas based on the common sedimentological features of the lahar deposits between nearby sites. On the other hand, distant sites with sedimentologically different deposits were fed from different source areas. These important constraints are used to validate and inform lahar numerical models (de' Michieli Vitturi et al., 2024) and simulations (Sandri et al., 2024) using a shallow layer approach for hazard assessment. We cannot rule out the possibility that lahar pulses from different source areas (Somma–Vesuvius vs. Apennines) might have overlapped and further aggraded in the open plain.

At several locations, we found erosional unconformities (Fig. 16a) between the lower and upper flow units (Fig. 16b), as well as between the pyroclastic and lahar deposits. Erosion is an important factor for the entrainment of pre-existing materials and objects, which include large-sized clasts external to the remobilized pyroclastic material. Size and density of the largest clasts embedded in the deposits can give an idea of the carrying capacity of the lahars.

Occurrences of large clasts and boulders are reported in the area invaded by both syn- and post-eruptive lahars, with a distribution that follows the one of the lahar deposits; in particular, both are found at the mouth of the valleys and in the alluvial plain. The presence of the erosional features (Fig. 16a), and the fact that the deposits are mostly composed of massive and relatively thick units (Fig. 16b), suggests that high sediment transport and deposition both occurred in the same area (Doronzo and Dellino, 2013; Roche, 2015). Such occurrences of erosion and accumulation of multiple units were useful to inform the lahar modeling of de' Michieli Vitturi et al. (2024).

We calculated local velocities of the syn- and post-eruptive Pollena lahars based on the biggest clasts that are found in the deposits at various stratigraphic heights, with boulder dimensions from several centimeters to a meter, and for flow density $\geq$ water density (Appendix A). The faster the lahar the higher the capability of its flow to entrain bigger external clasts. This occurred at locations where such clasts were freely available on the substrate or where the lahars impacted and damaged anthropogenic structures.

Then, we used the flow velocities (Fig. 17) to calculate local dynamic pressures of the lahars (Fig. 18) as a function of the clast properties (size, density, and shape). The obtained estimations are used by Sandri et al. (2024) to validate the probabilistic hazard assessment of lahars from Vesuvius eruptions.

The data presented in Figs. 17 and 18 represent minimum local values of the flow velocity and dynamic pressure, respectively, useful to assess some minimum impact of the lahars in the alluvial plain. An approximation of this point-by-point approach is that the values were calculated for the finding locations of the clasts in the deposits, meaning that the values are overestimated for those exact locations, while they should more properly be referenced to the immediate surroundings upstream. We did a parametric test to quantify

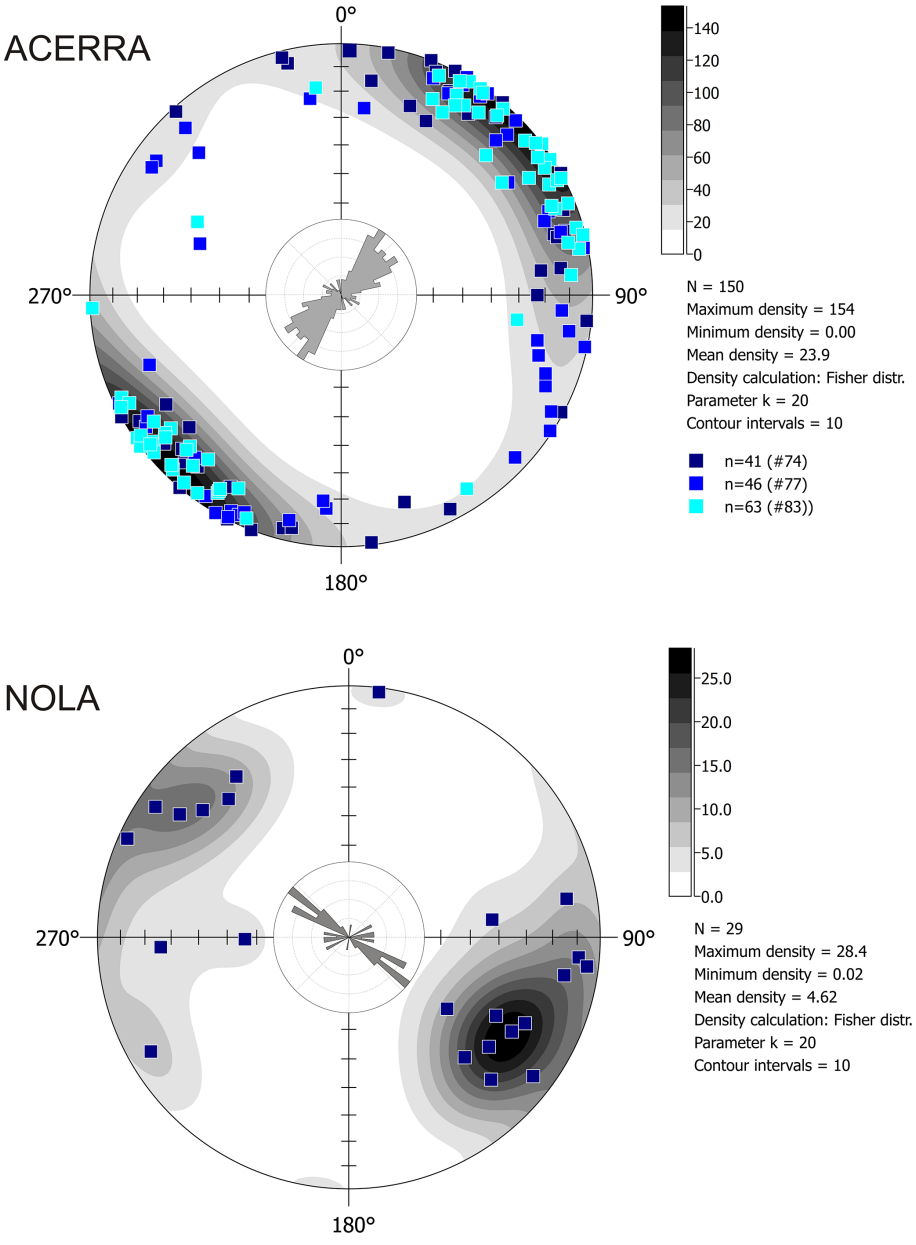

Figure 13. Equal-area projection and rose diagram of the K_1 directions at Acerra (12 km from Somma–Vesuvius) and Nola (10–15 km from Apennine source valleys).

the sensitivity for different physical states of the multiphase flow depending on initial fluidization and flow density, as well as considering two end members, from a non-fluidized case to an initially fluidized and non-expanded case (see Appendix A; Roche et al., 2013). From the performed analysis, we found that the most typical values refer to the initially fluidized and slightly expanded case (that is, a few percent more expanded than the non-expanded case), with most of the points falling in the velocity range of 2–4 m s^{-1} and dynamic pressure of 4–8 kPa.

Lastly, in eight locations we found the lahar deposits emplaced against meter-sized obstacles, from which we estimated, by comparison, local flow heights of the order of 1–1.5 m and particle volumetric concentrations of $\sim 30\,\%$ or more; i.e., the deposit thickness is $\sim 1/3$ of the lahar thickness (see Capra et al., 2018).

5 Discussion

The historical sources used as a benchmark for lahars around Somma–Vesuvius and in the Apennine valleys mark the fre-

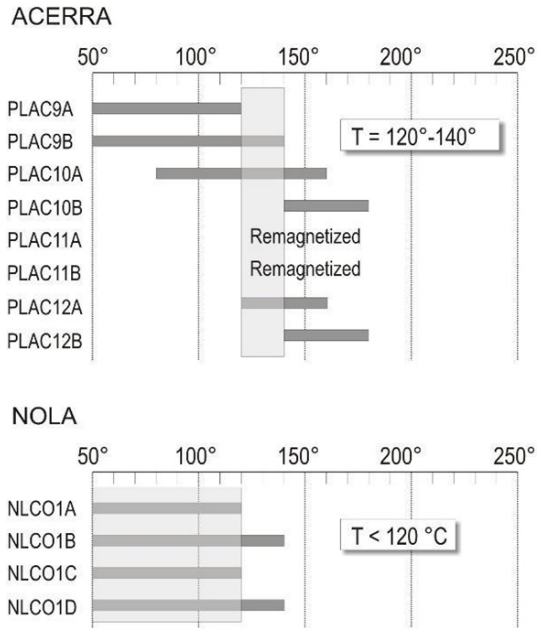

Figure 14. Deposition temperature at Acerra and Nola. The site T_{dep} is estimated from the overlapping reheating temperature ranges for all lithic clasts sampled.

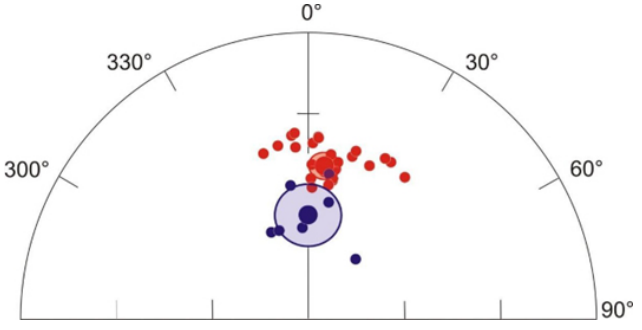

Figure 15. Equal-area projection of the characteristic remanent magnetization directions and their mean value with associated confidence limit from Acerra (red dots, mean value: $n = 26$ $D = 7.5°$, $I = 43.4°$, alpha95 = 3.5°) and Nola (blue dots, mean value: $n = 7$, $D = 0.8°$, $I = 60.2°$, alpha95 = 9.0°).

quent and broad impact that explosive eruptions of Vesuvius had in historical times. Some of the eruptions in the last 4 centuries (e.g., 1631, 1822, 1906, and 1944) impacted a number of municipalities, particularly during the sub-Plinian eruption of 1631. Heavy rain events caused remobilization of the primary pyroclastic deposits, triggering multiple lahars during or immediately after the eruption up to a few years (syn-eruptive lahars; Sulpizio et al., 2006); post-eruptive lahars were triggered on the longer term.

On the other hand, the Pollena eruption had an even wider impact in terms of both primary pyroclastic deposition and secondary (lahar) impact. For this event, historical sources are scarce to absent.

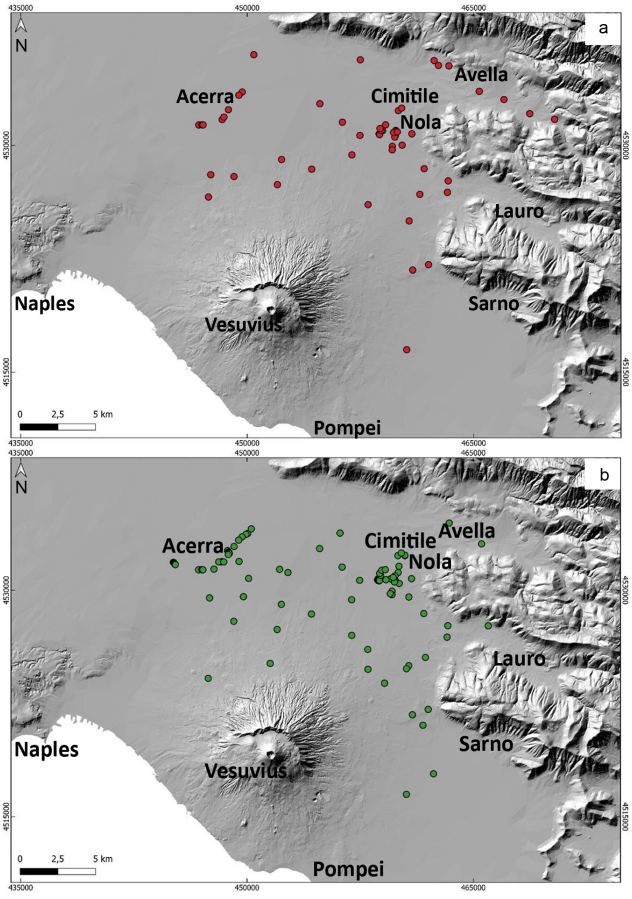

Figure 16. (a) Sites with evident erosion traces at the base of the lahar units. **(b)** Sites at which multiple depositional flow units are vertically identified. Both pieces of evidence corroborate the interpretation of the depositional mechanisms, as well as constraining the choice of the shallow layer approach for the lahar models and simulations (de' Michieli Vitturi et al., 2024; Sandri et al., 2024).

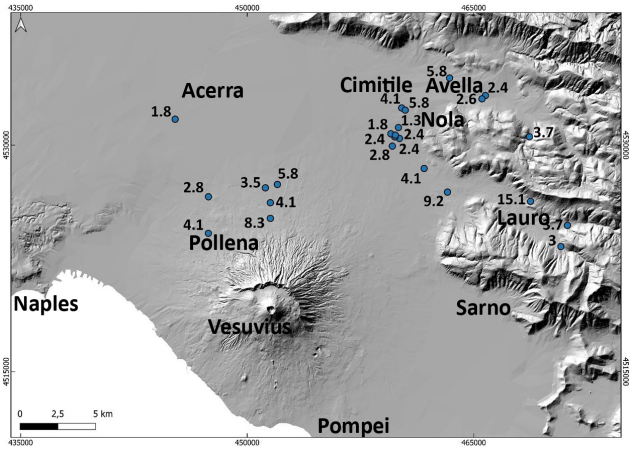

Figure 17. Average lahar velocities (in $m\,s^{-1}$) estimated with a point-by-point reverse engineering approach.

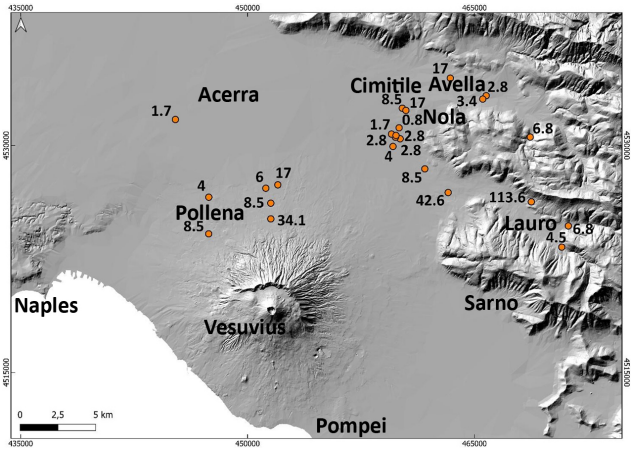

Figure 18. Average lahar dynamic pressures (in kPa) estimated with a point-by-point reverse engineering approach.

The analysis and realization of a database with more than 500 stratigraphic sections were done, which also includes the sedimentological features of the lahar deposits relative to the two sub-Plinian Vesuvius eruption case studies: Pollena and 1631. The detailed reconstruction and mapping of the primary deposits allowed us to update the area affected by pyroclasts dispersal, and it was found that both eruptions had an impact larger than previously known. In particular, the stratigraphic and sedimentological reconstruction of the deposits was done not only in the countryside but also close to urban areas, and this is important in terms of local impact of the lahars in the environment. Specifically, such impact investigation was done in urban areas including archeological findings (e.g., urban structures, walls).

These findings include not only new data from the Somma–Vesuvius plain, but also more distal data from Lauro Valley and Avella–Baiano Valley (Apennines), which were subjected to heavy remobilization of the primary deposits including the widely dispersed fine ash deposits formed in the late stage of the eruptions. Indeed, the accumulation areas that were reconstructed reveal an enlargement and extra 47 % (Pollena eruption) and 230 % (1631 eruption) coverage that was not previously known, and this should be considered in the hazard and impact evaluation in the Campanian Plain and on the nearby Apennine reliefs. The full database allows a more precise reconstruction of the new isopachs for both the Pollena and 1631 eruptions, which is possible given the high number of data points in the study area.

With particular reference to the lahar deposits, the syn-eruptive ones occurred by relatively short-term (during or immediately after the eruption) events and were directly emplaced on the primary pyroclastic deposits for both the Pollena and 1631 eruptions. Also, there are no significant erosion surfaces or humification traces in the sequences due to prolonged exposure of the primary deposits, demonstrating that the secondary emplacement was quite immediate (max a few years; Sulpizio et al., 2006) after or even during the eruption. The syn-eruptive features are also evidenced by the absence of anthropogenic traces or humified surfaces at the base of or interbedded in the lahar deposits, as further evidence of a very short-term time span between the eruptions and the lahar events. Another interesting feature is the presence of multiple depositional flow units, as evidenced by grain-size changes, some clast alignments, and concave erosion surfaces in the lahar deposits. Such depositional units were formed by en masse emplacement (with reference to single flow pulse), while the whole lahar deposits were formed by rapid progressive aggradation of the various flow units (Vallance and Scott, 1997; Doronzo, 2012; Roche, 2012; Smith et al., 2018; Martí et al., 2019; Guzman et al., 2020; see also Sulpizio et al., 2014, p. 56), which does not contradict the principle of superposition. This can be argued by the generally massive facies of each flow unit in the deposits and by the presence of water escape structures that vertically cross the entire deposit sequences. The latter evidence demonstrates rapid water loss through vertical escape "pipes" during or soon after the aggradation of the sequences. In other words, the various flow units (layers) must decouple from the transport system, and such decoupling occurs unit by unit and not particle by particle (Sulpizio et al., 2006, 2014; Roche, 2012; Doronzo and Dellino, 2013; Breard and Lube, 2017; Smith et al., 2018) through a massive accumulation rate (Duller et al., 2008; Doronzo et al., 2012; Martí et al., 2019).

The analysis of the Pollena lahar lithofacies allowed the identification of two main deposit categories. The first one occurs on an area that extends for more than 10 km north of Mount Somma, and the second one occurs on an area that extends west of the Apennines. For the latter, we can recognize two significant sub-categories of deposits, corresponding to the main valleys in the northwest–southeast direction: Avella–Baiano Valley and Lauro Valley. The difference between the first and the second deposit categories seems to reflect the types of primary deposits that were remobilized (fine ash vs. ash and lapilli). In the area north of Mount Somma, which also comprises the municipalities of Acerra and Afragola (about 12 km from Somma–Vesuvius), the primary lapilli fallout deposits are absent. In this part of the plain, the thin layer of phreatomagmatic ash is widely present, while thick fine-grained pyroclastic current deposits are present in the Mount Somma valleys that fed some of the lahars. In Avella–Baiano Valley and Lauro Valley, which also comprise the municipalities around Nola 10–15 km from Apennine source valleys (Fig. 1 and Appendix C), the lahar deposits are generally coarser and consist of multiple depositional units with different lithofacies (Table 3). In this case, both grain size and componentry indicate that lahar deposits resulted from the remobilization of the fallout deposits. Such considerations also derive from the full compilation of the geospatial database. A volume estimation of the remobilized syn-eruptive deposits, based on a QGIS cal-

Table 3. Statistical parameters (mean and sorting) extracted from the grain-size analyses and reference lithofacies (see Table 2 for descriptions).

Sample	Mean (φ)	Sorting (φ)	Lithofacies
Lauro Valley			
T17-01	−0.93	1.41	Gms
T17-02	−1.83	1.23	Gms
T17-03	2.42	1.46	Sh
T15-05	−1.39	1.74	Gms
T47-04	1.67	1.61	Mm
T118-01	1.13	2.7	Gms
Avella–Baiano Valley			
T10-02	−0.78	1.47	Sh
T8bis-02	0.31	1.83	Sh
T3-04	−0.95	1.83	Gms
IM-CM3-01	−1.13	1.54	Gms
IM-CM3-02	−0.48	1.35	Gms
IM-CM1-01	−1.66	0.86	Gms
IM-CM1-02	−1.17	1.62	Gms
IM-CM1-03	−1.13	1.83	Gms
IM-CM1-04	0.06	1.39	Fm
US-55	−0.84	1.97	Gms
US-56	1.17	1.8	Sh
US-57	−1.51	1.86	Gms
US-49	0.69	2.16	Gms
US-127	−1.66	1.39	Gms
US-127A	−1.02	2.23	Gms
US-128	−1.72	1.91	Gms
IM-NL1-02	−0.5	2.49	Gms
IM-NL1-03	1.25	2.1	Gms
IM-NL1-04	2.99	0.89	fM
IM-NL1-05	2.64	1.20	fM
Somma–Vesuvius			
AC3_96-02	2.37	1.26	mM
AC3-98	2.48	1.2	mM
AC_BON	3.52	0.38	mM
T123-02	1.37	1.5	mM

culation, is 7×10^7 m^3 for the northern Vesuvius area and 4×10^7 m^3 for the Lauro Valley.

Referring to the 1631 eruption, previous maps have shown the distribution of the 1631 lahar deposits toward east, basically following the distribution of the primary pyroclastic fall deposits (Sulpizio et al., 2006), while in Figs. 10 and 11 we show a significantly larger distribution area, particularly toward the north (Somma–Vesuvius ramps and plain) and east (Apennines valleys), and less toward the southeast. In particular, this distribution is well-explained by the wide distribution of the ash fallout deposit toward both north and northeast (Fig. 6), remobilized during the lahar generation from both the Mount Somma and Apennine slopes. On the other hand, looking at the average deposit thicknesses, they reach half a meter in the north and northeast, while they reach a couple of meters in some locations in the northeast (aligned with the dispersion axis of the primary fallout deposits and out of the Apennine valleys).

The sedimentological analyses carried out on a number of samples from the different studied sectors (Somma–Vesuvius, Lauro Valley, Avella–Baiano Valley) are useful for discriminating the various factors that contributed to the initiation of the lahars and emplacement of their deposits. The samples from Lauro Valley and Avella–Baiano Valley are coarser (but have a significant finer tail) than the ones for Somma–Vesuvius, and this can depend on three factors: (i) genetic types of the primary pyroclastic deposits (fall vs. flow), (ii) interaction between lahars and morphology (valley vs. plain), and (iii) major remobilization in Lauro Valley and Avella–Baiano Valley of the distal phreatomagmatic fine ash deposits formed in the late eruption stages. In other words, the primary grain sizes involved in the remobilization (finer and higher-water retention for Somma–Vesuvius), as well as the general topography (gentler but longer ramp for Somma–Vesuvius), likely acted as the main factors directly impacting the distribution of the lahar deposits and the decay of the flow velocities and dynamic pressures in the area.

Interestingly, an emplacement temperature of $\sim 120\,^{\circ}$C of the lahar deposits was calculated for those generated along the Somma–Vesuvius slopes, indicating a relatively hot provenance after remobilization of the pyroclastic current deposits. Instead, the remobilization from the Apennine sectors involved only cold fallout deposits. The companion paper of de' Michieli Vitturi et al. (2024) also investigates the nexus between water temperature, flow viscosity, and their consequential impact on fluid dynamics. Specifically, when the dominance of frictional forces is attributable to the yield slope term, the initial divergence between high- and low-temperature scenarios appears negligible. However, discernible dissimilarity appears over time for the inundation area of the colder flow case (i.e., 27 °C) with respect to the warmer counterpart (i.e., 100 °C), the latter case being close to the 120 °C reported from paleomagnetism. Remarkably, the temperature-induced variations assume a pivotal role in shaping the dynamic characteristics of the hotter flow. The diminished viscosity associated with elevated temperatures not only amplifies fluid mobility but also prompts a notable acceleration in sediment settling velocity. This, in turn, initiates a debulking mechanism, thereby intensifying overall flow mobility. Consequently, this intricate interplay contributes to a reduced footprint of deposited material from the flow, altering the spatial distribution of sediments. However, the overall impact on the inundation area is typically quite reduced, typically being less than 10 %–20 % even considering a thickness threshold of 1 mm (see de' Michieli Vitturi et al., 2024). The sampled clasts might have been incorporated multiple times by the flows, and the heating–cooling processes that we interpret as indicating T_{dep} in the diagrams are the last to have occurred and affected the samples. Be-

sides, a third heating component is clearly observed for some of them. The paleomagnetic directions are statistically distinguishable, supporting the idea that the lahar emplacement at Nola (10–15 km from Apennine source valleys) and Acerra (12 km from Somma–Vesuvius) was not synchronous, as further evidence of the different timing and hence likely different detachment areas involved during the pyroclast remobilization. However, the comparison with the paleosecular variation curves of the Earth's magnetic field does not allow better constraining the entity of the time span between the two lahar events. The parental lahars acted as mass flows capable of entraining outsized clasts (where available) from substrate under the action of shallow layer flow velocity and dynamic pressure (de' Michieli Vitturi et al., 2024), then emplaced massive flow units with uplifted external clasts set into the much finer matrix (see Roche, 2015). In some lahar units, various clasts have been found, showing some alignment that depends on the mechanisms of entrainment and uplift (with respect to substrate) within the flow.

In terms of local impact in the Pollena case study (the largest one), while most of the calculated points (44) fall in the range of lahar velocity of 2–4 $m\,s^{-1}$ and dynamic pressure of 4–8 kPa, a few peak velocity values of 13–15 $m\,s^{-1}$ and dynamic pressure of 90–115 kPa are also calculated, which are directly related to meter-sized clasts entrained into the lahars on the steep slopes, then deposited downstream of alluvial fans. Such values of the velocity and dynamic pressure are comparable with those calculated for lahars that occurred recently at Ruapehu in 2007 (Lube et al., 2012) and Merapi in 2011 (Jenkins et al., 2015), as well as in historical times at El Misti (Thouret et al., 2022). In particular, the estimated velocities and pressure agree with those of Lube et al. (2012) and Jenkins et al. (2015). Moreover, multiplying velocity and density gives a power per unit surface, so those most representative values correspond to a flow power per unit surface of 8×10^3–3.2×10^4 $W\,m^{-2}$, with peak values of 1.17×10^6–1.72×10^6 $W\,m^{-2}$, in agreement with typical values reported for floods and megafloods (Russell and Knudsen, 1999; Whipple et al., 2000; Carling, 2013).

6 Conclusions

The integration of the historical, stratigraphic, sedimentological, laboratory, and impact parameter analyses carried out in the Vesuvius area allow updating the lahar invasion related to the Pollena and 1631 eruptions. In general, the physical characteristics of the analyzed deposits indicate that syn-eruptive lahars are related to the rapid remobilization of large volumes of pyroclastic material, which is mainly fine-grained and almost exclusively derived from the accumulation of products related to a single eruption. The analysis also shows that tardive (post-eruptive) mass flows are common and involve multiple and variably altered deposits, and it shows that their energy and frequency are progressively lower over time after the last eruption has occurred. In particular, a higher impact from both primary and secondary phenomena is something that should be accounted for in the Vesuvius area, in addition to the following.

- The new isopach maps of the Pollena and 1631 eruptions allow us to infer a larger impact than previously known for these two sub-Plinian events of the Vesuvius. Thus, it is worth reconsidering the territorial impact that sub-Plinian eruptions can have in the Vesuvius (but not only) area. In particular, the ash deposits can have a high impact in relation to their high density and low permeability.

- The primary impact from fallout and pyroclastic current processes in the Vesuvius area was – and may be in the future – followed by the secondary impact from lahars generated during or immediately after the eruption events. Both impacts can have a wide distribution because they are directly controlled by the primary deposit distributions both around Somma–Vesuvius and in the Apennine valleys.

- The runouts of such lahars were significant for both the Pollena and 1631 eruptions by reaching distances of 10 to 15 km from the sources, and their deposit geometry is tabular-like with average thicknesses of 0.5 to 1 m.

- The paleotemperature data highlight relatively hot dynamics (~ 120 °C) for those lahar flow pulses that traveled down the Somma–Vesuvius slopes because of pyroclastic current deposit remobilization. This did not occur from the Apennine sectors, where pyroclastic currents did not reach, and only cold fallout deposits were remobilized.

- A reverse engineering approach allowed us to calculate the local lahar velocities (2–4 $m\,s^{-1}$, with peaks of 13–15 $m\,s^{-1}$), dynamic pressures (4–8 kPa, with peaks of 90–115 kPa), and solid volumetric concentration (~ 30 %, implying a 1 : 3 ratio between deposit and flow thickness) on the basis of the external clast properties entrained into the flows then emplaced into the ash matrix and based on the presence of the lahar deposits in proximity to obstacles and archeological findings.

As a general conclusion, we have demonstrated that the areal impact of both primary deposits and lahars, in the case of sub-Plinian events at Somma–Vesuvius, involves a territory wider than previously known and for several years, with possible decreasing damage over time.

Appendix A: Calculation of lahar velocities and dynamic pressures

A theoretical scheme is presented to quantify local velocities and dynamic pressures of the lahars by inverting the field fea-

tures at selected locations. The final goal is to map the values of velocity and dynamic pressure to assess the hazard from lahars in the study area. Flow dynamic pressure, P_{dyn}, results from a combination of flow density, ρ_f, and flow velocity, v, and is defined as

$$P_{dyn} = 0.5\rho v^2. \quad \text{(A1)}$$

In the study area, the original flow was a multiphase flow of water + pyroclastic sediment, which during remobilization evolved into a flow of water + pyroclastic sediment + external clasts. Generically, flow density results from a combination of particle density, ρ_p, and water density, ρ_w, through particle volume concentration, C, and is defined as

$$\rho_f = \rho_p C + \rho_w(1 - C). \quad \text{(A2)}$$

In order to define flow velocity, we take into account stratigraphic and sedimentological characteristics of the lahar flow units: (i) they are ubiquitously massive and result from remobilization of the primary pyroclastic deposits, then emplacement from mass flows; (ii) they contain big external clasts entrained (by dynamic pressure) and uplifted (also by pore pressure) from substrate into the flows. With these field characteristics, flow velocity can be expressed as a combination of entrained clast properties and flow density and is defined as (modified after Roche, 2015)

$$v = \sqrt{\frac{X\psi\,(\rho_c - \rho_w)\,g}{\gamma\rho_f}}, \quad \text{(A3)}$$

where X is clast small axis, ψ is clast shape factor, ρ_c is clast density, g is gravity acceleration, and γ is an empirical constant. Equation (3) allows quantifying the incipient motion of the big clasts and gives minimum values of flow velocity required to entrain and uplift the clasts from substrate, probably more than once, before being emplaced into the lahar deposits by flow velocity drop. The equation was originally derived in laboratory experiments for a multiphase flow of air + sediment and performs highly at $\rho_f \sim 1000\,\mathrm{kg\,m^{-3}}$ (hindered settling) for dense pyroclastic currents controlled by topography then opened to an alluvial plain (Martí et al., 2019), which is a case similar to the lahars in the study area. Substituting Eq. (3) into Eq. (1) and simplifying gives

$$P_{dyn} = 0.5\frac{X\psi\,(\rho_c - \rho_w)\,g}{\gamma}. \quad \text{(A4)}$$

For given clast properties, flow dynamic pressure has a unique value, while flow velocity is a function of flow density. Indeed, the present scheme is a spot model that basically depends on, and is limited to, the finding of big clasts and boulders within the lahar deposits. An approximation is that velocity and dynamic pressure are calculated for the locations where the clasts are found in the deposits, meaning that the calculated values are overestimated for those exact locations, while they are more properly referenced to the immediate surroundings upstream.

At the selected locations in the study area, we collected the dimensions of the biggest clasts found in the lahar deposits, and we lithologically characterized the clasts in the field to calculate flow dynamic pressures using Eq. (4). We used the following values for the various parameters in the calculations: ψ (ellipsoid) = 0.66; ρ_c (limestone) = $2500\,\mathrm{kg\,m^{-3}}$; ρ_c (ceramic) = $2000\,\mathrm{kg\,m^{-3}}$; ρ_c (brick) = $2000\,\mathrm{kg\,m^{-3}}$; ρ_c (tephra) = $1500\,\mathrm{kg\,m^{-3}}$; ρ_c (lava) = $2500\,\mathrm{kg\,m^{-3}}$; ρ_c (iron) = $8000\,\mathrm{kg\,m^{-3}}$; $\rho_w = 1000\,\mathrm{kg\,m^{-3}}$; $g = 9.81\,\mathrm{m\,s^{-12}}$; $\gamma = 0.031$–0.071. Also, we calculated flow velocities using Eq. (3) in the following range of flow density: $\rho_w \le \rho_f \le \rho_p$, where $\rho_w = 1000\,\mathrm{kg\,m^{-3}}$ and $\rho_p = 2000\,\mathrm{kg\,m^{-3}}$. In this way, flow density spans from two extreme cases: (i) $\rho_f = \rho_w$, which means negligible pyroclastic sediment and external clasts, so water flow only; and (ii) $\rho_f = \rho_p$, which means negligible water and dominant pyroclastic sediment, so ash flow only. For the empirical constant in Eq. (3), we used three different values to test the sensitivity with respect to different physical states of the multiphase flow: γ (non-fluidized) = 0.031; γ (initially fluidized and slightly expanded) = 0.057; γ (initially fluidized and non-expanded) = 0.071 (see Roche et al., 2013; Fig. A1).

Regarding flow velocity, after calculation we can rewrite Eq. (3) in a simpler form (to more directly relate velocity to density) as follows

$$v = \frac{a}{\sqrt{\rho_f}}, \quad \text{(A5)}$$

where $a > 0$ depends on clast properties, and its square has dimensions of pressure. On the other hand, it is not straightforward to constrain local flow velocities with unique values of flow densities, mostly because small variations of velocity correspond to large variations of density, and this is particularly valid for volcaniclastic mass flows (Carling, 2013; Jenkins et al., 2015; Roche, 2015; Martí et al., 2019; Guzman et al., 2020; Thouret et al., 2022).

At some locations in the study area, we found lahar deposits against meter-scale manufacturing obstacles (Di Vito et al., 2009). The peculiarity is that the deposits in proximity to the obstacles are thicker than the correlated ones in the free field but never reach the top of the obstacles themselves. This means that the lahars were not very expanded, so they were unable to overcome the obstacles as stratified flows would have done (see Spence et al., 2004; Gurioli et al., 2005; Doronzo, 2013; Breard et al., 2015). With this field evidence, we can assume that local flow height, H, was similar to deposit thickness against the obstacle, h_o, as

$$H \approx h_o. \quad \text{(A6)}$$

In order to estimate flow density using Eq. (2), we focus on particle volumetric concentration. For well-sorted deposits, such concentration can be defined with an average value over

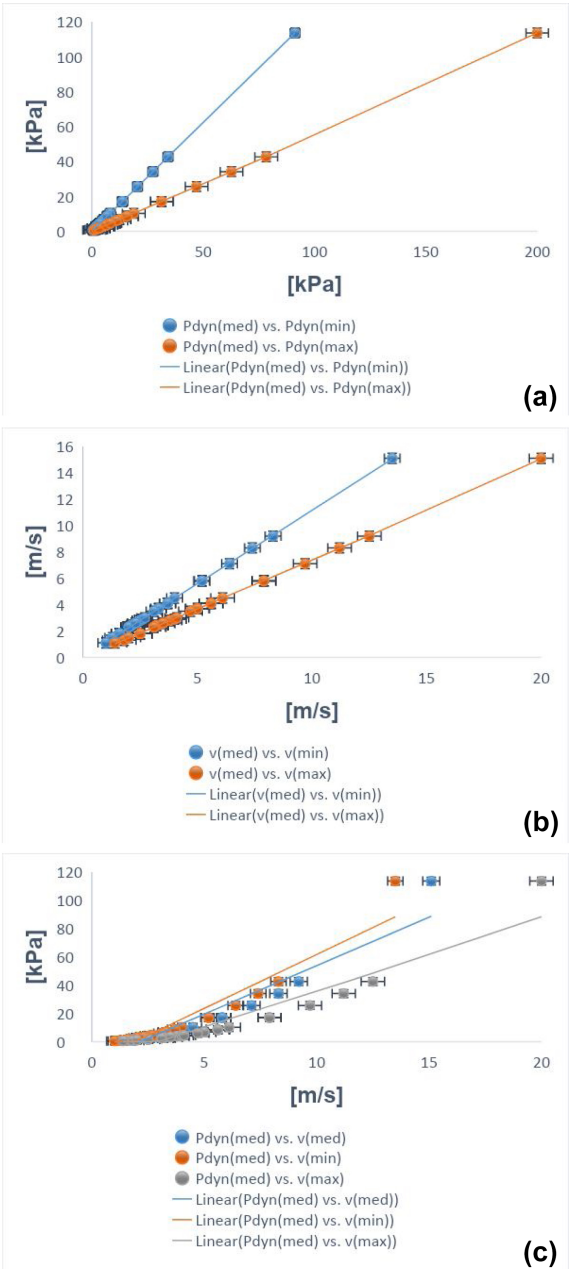

Figure A1. Local dynamic pressures and velocities for the syn- and post-eruptive Pollena lahars calculated with the reverse engineering approach. **(a)** Dynamic pressure for the initially fluidized and slightly expanded case vs. dynamic pressure for the initially fluidized and non-expanded (blue) and non-fluidized (orange) cases; **(b)** velocity for the initially fluidized and slightly expanded case vs. velocity for the initially fluidized and non-expanded (blue) and non-fluidized (orange) cases; **(c)** dynamic pressure for the initially fluidized and slightly expanded case vs. velocity for the initially fluidized and slightly expanded (blue), vs. velocity for the initially fluidized and non-expanded (orange), and vs. velocity for the non-fluidized (gray) cases.

flow height as follows (modified after Doronzo and Dellino, 2013; see also Eq. 30 in de' Michieli Vitturi et al., 2024):

$$C = \frac{h_f}{H}, \tag{A7}$$

where h_f is deposit thickness in the free field. Substituting Eq. (6) into Eq. (7) gives

$$C \approx \frac{h_f}{h_o}. \tag{A8}$$

In particular, h_f refers to lahar deposits relatively close to the obstacles but which were not affected by them during emplacement, i.e., close but not so much. We assessed that correlation taking into account the stratigraphic and sedimentological characteristics of the lahar deposits and the fact that Eq. (7) performs better with layers emplaced after remobilization of primary pyroclastic fallout or dominantly ash flow deposits.

Lastly, we macroscopically assessed erosion in the field by characterizing the unconformities present in both the primary pyroclastic and lahar deposits. In particular, the syn-eruptive lahar deposits consist of more than one flow unit, so it is important to understand how the different flow pulses interacted with each other during emplacement. The main unconformities that are found in the field are attributed to the partial absence of a flow unit and the loss of lateral continuity despite some flat geometry of the deposits. On the other hand, at some locations we were not able to assess if erosion occurred or not due to multiple open issues: (i) possible absence of the primary pyroclastic deposits, (ii) possible exclusive presence of the post-eruptive lahar deposits, and (iii) impossibility to get to some outcropping deposit base and possible unconformities.

Appendix B: Paleo-temperature and paleo-direction determinations

The magnetic fabric of a deposit was investigated by measurements of the magnetic susceptibility and its anisotropy (AMS). AMS was measured with a Kappabridge KLY-3 (AGICO), and data were elaborated by the software Anisoft5 (AGICO). AMS depends on the type, concentration, and distribution of all the minerals within the specimen. It is geometrically described by a triaxial ellipsoid, whose axes coincide with the maximum (k_1), intermediate (k_2), and minimum (k_3) susceptibility directions. The magnetic fabric of a specimen is then described by the direction of the k_1 axis, the magnetic lineation (L), and that of the k_3 axis, which is parallel to the pole of the magnetic foliation plane (F). Besides, the modulus of the susceptibility axes provides some magnetic parameters useful to express the intensity of the anisotropy (P_j) and the oblate–prolate fabric occurrence (T). Generally, sedimentary vs. pyroclastic deposit fabric, here considered to be a proxy for the lahar fabric, is oblate with a horizontal

to gently imbricated (less than 20°) magnetic foliation. The magnetic lineation is normally clustered along the foliation plunge. In this case, both the F imbrication and the L direction can provide the local flow direction. Other times, L is orthogonal to the F plunge or F is statistically horizontal, and it is not possible to infer the flow direction.

For T_{dep} estimation, pottery shards were subjected to progressive thermal demagnetization (PTD), with heating steps of 40 °C, up to the Curie temperature (T_C), using the Schonstedt furnace and the spinner magnetometer JR6 (AGICO). The rationale of the method has been described in detail in several papers (McClelland and Druitt, 1989; Bardot, 2000; Porreca et al., 2007; Paterson et al., 2010; Lesti et al., 2011), many of them dedicated to pyroclastic density currents (PDCs) of the Vesuvius area (Cioni et al., 2004; Di Vito et al., 2009; Giordano et al., 2018; Zanella et al., 2007, 2018, 2015). Typically, measurements are made on accidental lava lithics that were entrained during pyroclastic or lahar flows. In this case, we had the opportunity to estimate the T_{dep} by measuring ancient pottery artifacts. Briefly, pottery is characterized by a thermal remanent magnetization (TRM) acquired during its manufacture and its subsequent history of daily use. Whenever it is heated, part of its TRM, the one associated with blocking temperatures (T_b) below the heating one (T_h), is overwritten. Without alteration phenomena, the heating–cooling is a reversible process, except for the magnetic directions. The original TRM shows a random paleomagnetic direction due to the transport during emplacement. Subsequent TRMs show directions parallel to the Earth's magnetic field during their cooling. This is clearly illustrated in the Zijderveld diagrams. The composition of the different magnetization components reveals thermal intervals characteristic of the heating history of the potsherd. Of course, this explanation is simplified, but the method is well-established and has been shown to work well with heated artifacts, such as in the case of tiles and pottery embedded in the PDC deposits at Pompeii (Gurioli et al., 2005; Zanella et al., 2007), Afragola (Di Vito et al., 2009), and Santorini (Tema et al., 2015). In the case of a lahar, we expect low T_{dep} or cold deposits. This can be a major concern because of the difficulties distinguishing between the TRM secondary components and the chemical (CRM) and viscous (VRM) remanent magnetization. The CRM may develop due to mineralogical changes during reheating (McClelland, 1996). Instead, VRM is typical of ferromagnetic grains with low T_b and often occurs in most rocks. Following the Bardot and McClelland (2000) relationship for time intervals in the 10^2–10^6-year range with $T_b = 75 + 15$ log (acquisition time in years) and using the Pollena eruption date (472 CE), we obtain a lower limit of the T_b around 123 °C. This means that this temperature helps us discriminate between "hot" ($T_b > 120$ °C) and "cold" lahars ($T_b < 120$ °C).

Finally, routine magnetic measurements were done on the lahar matrix to determine the characteristic remanent magnetization (ChRM) by thermal and alternating field demagnetizations. The direction of the Earth's magnetic field during the Pollena eruption is well-known (Zanella et al., 2008). If the sampled lahars were emplaced shortly after the eruption, both the secondary TRMs and the matrix of the lahars should show a remanent magnetization direction similar to the Pollena ones. ChRMs can also test if the two lahars (Acerra at 12 km from Somma–Vesuvius and Nola at 10–15 km from Apennine source valleys) are coeval.

Appendix C: Description of the studied areas

C1 Area 1 – Nola

In the area surrounding Nola (10–15 km from Apennine source valleys), it is possible to recognize the complete fallout sequence of the Pollena eruption (*a* in Figs. C1 and C2), which usually covers plowed soils (*p* in Fig. C1) and late Roman archeological remains. The sequence is composed of an alternation of coarse pumice and thin ash fallout layers. Its top is always made of a fine ash bed related to the phreatomagmatic phase of the eruption (*b* in Figs. C1 and C2), with a thickness ranging from 1 to 14 cm due to erosion. They are almost always overlain by lahar deposits composed of several flow units (*c* in Figs. C1 and C2) with large thickness variability due to channeling and the presence of barriers and buildings. They sometimes include blocks, tiles, and other archeological remains.

In Fig. C1, above the primary deposit, there is an example of a well-exposed sequence composed of at least five units (*c* in Fig. C1). The first one is a massive and matrix-supported deposit composed of fine and non-vesiculated ash (lithofacies Gms), with fragments of greenish to blackish scoriae and minor fragments of pumices, lavas, and limestones. The fragments are centimeter-sized and are both angular and rounded. The second flow unit is similar to the one below but is darker and contains less coarse fragments. Its matrix is composed of an alternation of fine to medium ash layers. It follows a plane-parallel sequence of well-sorted fine sand and silt layers characterized by the lithofacies fM. A massive deposit follows upward; it is progressively humified and contains abundant reworked and rounded pumice clasts from the Avellino eruption. The top humified surface is almost always eroded by anthropogenic activity and is generally plowed (*p*1 in Fig. C2). It is overlain by the primary deposits of the 1631 eruption (*d* in Fig. C2). It is few centimeters thick and is composed of a basal layer of dark coarse ash (small pumice fragments), overlain by a massive ash bed, containing abundant accretionary lapilli. The following deposit thickens in the plowing furrows and depressions, is composed of massive fine ash beds that are vesiculated and cohesive, and is interpreted as a lahar deposit (lithofacies mM) (*e* in Fig. C2). This deposit (*e* in Fig. C3) overlies the foundations of Palazzo Orsini (blocks in Fig. C3), which is now the seat of the Court of Nola and was built in the second half of the fifteenth cen-

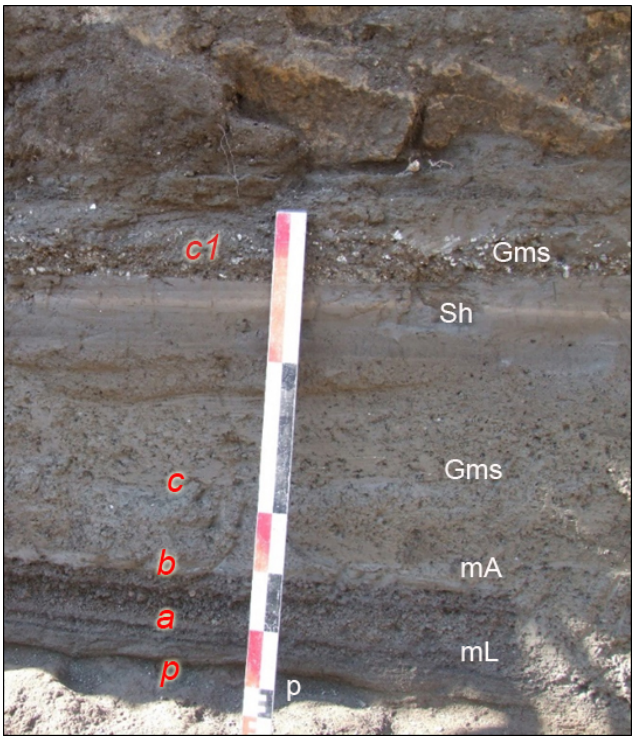

Figure C1. Nola (10–15 km from Apennine source valleys); Pollena fallout deposits overlain by at least five lahar units. In particular, *p* indicates paleosol, *a* indicates alternation of coarse and fine fallout sequences of the Pollena eruption, *b* indicates final ash fallout of the eruption, *c* indicates the sequence of syn-eruptive lahars, and *c*1 indicates a post-eruptive lahar containing white pumice fragments of the Pomici di Avellino eruption. For the description of lithofacies see Table 2.

tury (Fig. C3). The top is always eroded by modern anthropogenic activity and locally by deposits of recent eruptions of Vesuvius (e.g., 1822, 1906).

In Nola and in nearby Cimitile (about 10–15 km from Apennine source valleys), the effects on the territory of the lahar emplacement related to the Pollena eruption are testified by numerous archeological remains. The Nola and Cimitile areas are covered by thick sequences of fallout and lahar deposits. In fact, the previous ground level was at least 2–3 m below the present one. This effect is clearly visible in the Amphitheater Laterizio, which was completely filled by the primary and secondary deposits. The same is true in Cimitile, where at the archeological site of the early Christian basilicas the present ground level is about 2 m higher than the one before the eruption. It is worth noting that in Cimitile the flows were able to carry limestone blocks of 50 cm in diameter, likely along the main flow direction of the lahars (Fig. C4).

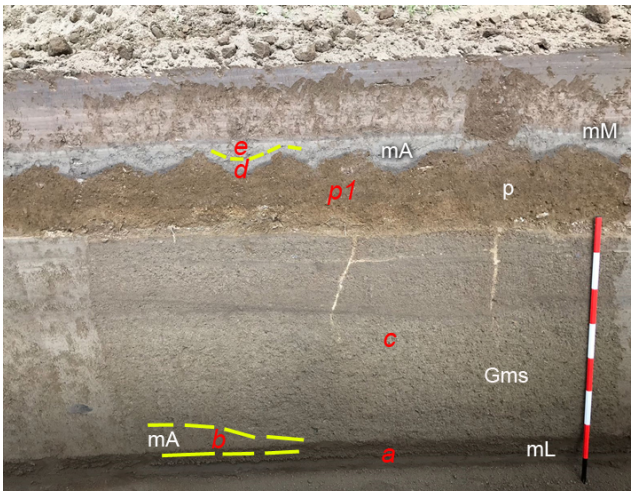

Figure C2. Nola (Pollena) lahar deposits overlain by a cultivated paleosol and by the 1631 ash fallout and lahars. In particular, *a* indicates alternation of coarse and fine fallout sequences of the Pollena eruption, *b* indicates final ash fallout of the eruption (partially eroded), *c* indicates a sequence of three lahar units, *p*1 indicates plowed paleosol, *d* indicates 1631 ash fallout deposits mantling the undulated paleosol, and *e* indicates a lahar deposit composed of a massive ash layer. For the description of lithofacies see Table 2.

Figure C3. Palazzo Orsini (Nola; 1631 fallout and lahars). In particular, *d* indicates 1631 ash fallout deposits overlying the foundations of the building (in the inset), and *e* indicates a syn-eruptive lahar deposit. For the description of lithofacies see Table 2.

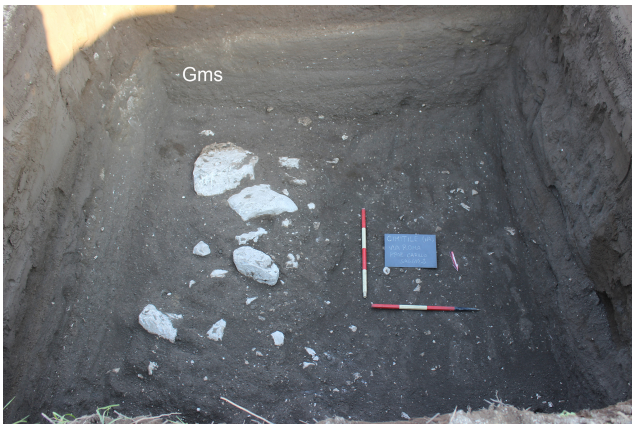

Figure C4. Cimitile; sequence of 3 m thick syn-eruptive lahar units with evidence of the transport of calcareous blocks (up to 50 cm). The largest are in the lower unit. The base of the lahar sequence and the underlying fallout deposit of the Pollena eruption are not visible in the photo. For the description of lithofacies see Table 2.

Figure C5. Acerra (12 km from Somma–Vesuvius); lahar deposit (unit 2) overlaying a cultivated paleosol (unit 3). The index finger indicates a water escape structure crossing the sequence of lahars. For the description of lithofacies see Table 2.

C2 Area 2 – Acerra–Afragola

The Acerra and Afragola territories (about 12 km from Somma–Vesuvius) are located north and northwest of Vesuvius and are almost flat areas crossed by the Clanis river. Both the coarse fallout deposits of the Pollena and 1631 eruptions are absent in this area. Here, only a thin, centimetric ash bed overlies the late Roman paleosol. This fine ash bed, which we correlate with the final phreatomagmatic phases of the Pollena eruption, is homogeneous and cohesive, and it mantles the ground without any significant lateral variation. The overlying deposit is characterized by high thickness variations; it is generally massive and contains vesicles from circular to flattened and coated by fine ash. It has a matrix-supported texture and is composed of fine to very fine, very cohesive ash and contains scattered and more or less abundant pumice and lithic fragments (lithofacies mM) as well as remains of vegetation (Stanzione et al., 2023). From one to three depositional units have been recognized, marked by unconformities and differences in grain size or color. The uppermost unit always contains white pumice fragments of the Avellino eruption. Drying-out structures and water escape structures are very common, which are vertical structures (Fig. C5) that look like fractures a few centimeters large, filled by finer material transported by the escaping water, formed soon after the emplacement of the sequence of the syn-eruptive lahars (Fig. C5). The maximum thickness recorded in this area is about 90 cm.

The top is almost always horizontal due to erosion related to modern anthropogenic activity, and only in a few exposures it is capped by a paleosol, with traces of human presence of Medieval times and of the deposits of the 1631 eruption as well. The base of this latter deposit is a centimeter-thick fine ash bed with an internal plane-parallel layering emplaced by fallout. It underlies a massive deposit with high thickness variations (max 20 cm) at the outcrop scale. It is composed of fine ash, is cohesive and vesiculated, and contains scattered small pumice fragments (lithofacies mM). The pumice fragments are vesicular, dark gray to blackish, and highly porphyritic with leucite, pyroxene, and feldspar crystals. The stratigraphic position and lithology confirm their attribution to the 1631 primary and secondary (lahars) deposits.

C3 Area 3 – Pomigliano–Marigliano

This area is located along the northern outer part of the Vesuvius apron (Santacroce et al., 2003). The studied sequences start from the paleosol developed on top of the ash deposits of the 79 CE eruption. The paleosol is mature and contains pottery fragments until the second century CE. Its top is undulated with traces of plowing spaced about 50 cm (*a* in Fig. C6). Representative sequences of the area include a basal ash layer with a thickness ranging from 1 to 4 cm (*b* in Fig. C7), thickening in the depressions, that is cohesive and locally vesiculated. It is interpreted here as co-ignimbritic ash emplaced by fallout during the phreatomagmatic final phases of the Pollena eruption. Upwardly, the sequence includes several lahar units from massive to slightly stratified, composed of fine and very cohesive ash, and containing scattered greenish pumice fragments (lithofacies mM) (*b*1 in Fig. C7). Locally, this deposit, also in the case of multiple units, is cut by vertical drying cracks. The sequence is overlain by a 25–30 cm thick mature paleosol, containing cultivation traces and majolica fragments (*c* in Figs. C6 and C7).

The top of this paleosol is undulated and covered by the primary deposit of the 1631 eruption (*d* in Fig. C7). The latter is represented by a discontinuous medium to fine ash

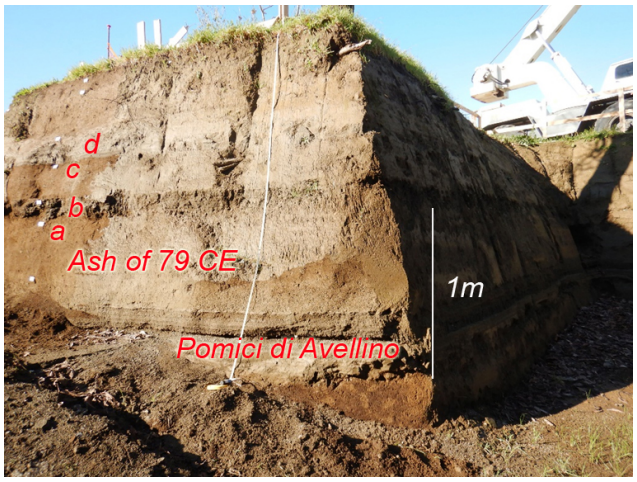

Figure C6. Pomigliano; sequence of deposits including (from bottom to top) Bronze Age paleosol, Pomici di Avellino (unit EU 5 of Di Vito et al., 2009), and paleosol developed on top of Pomici di Avellino and buried by the Pollena eruption deposits. In the central part, fine ash deposits of the 79 CE eruption are visible. The top of the paleosol is undulated and plowed. In particular, *a* indicates paleosol of Roman age, *b* indicates primary and secondary deposits of the Pollena eruption, *c* indicates paleosol between the Pollena and 1631 deposits, and *d* indicates 1631 primary and secondary deposits. Further details are in Fig. C7.

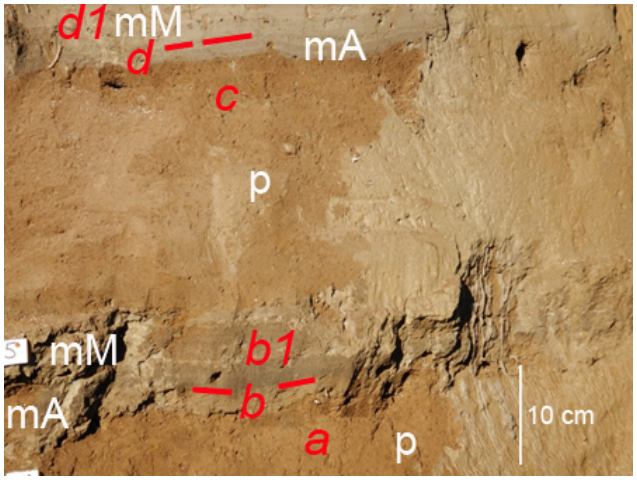

Figure C7. Pomigliano of Fig. C6: *a* indicates paleosol-containing potteries of the second century CE, *b* indicates ash deposit of the Pollena eruption, *b*1 indicates syn-eruptive lahars of the Pollena eruption, *c* indicates paleosol between Pollena and 1631, and *d* indicates primary deposits of the 1631 eruption overlain by syn-eruptive lahars (*d*1). For the description of lithofacies see Table 2.

layer, slightly laminated for contrasting grain size, up to 5 cm thick, with a gray to violet color, and containing dark pumice fragments and loose crystals of leucite, pyroxene, and biotite (Fig. C7). Its thickness variation is due to both slight internal variations (thickening in correspondence with depressions) and erosion by the following lahars. The latter are composed of one to three flow units (*d*1 in Fig. C7), with a cumulative total thickness varying from 10 to 45 cm. They are composed of massive fine and very cohesive ash and contain rare scattered dark pumice fragments similar to those of the 1631 eruption (lithofacies mM). These sequences are overlain by recently cultivated soil. Locally, thin ash beds of recent Vesuvius activity (like 1822, 1906) overlie the 1631 deposits.

C4 Area 4 – Avella–Baiano Valley

We have analyzed several sequences along the Avella–Baiano Valley, both exposed and excavated for the present work. Here the sequences of primary deposits are often affected by deep erosion; in fact, in some places the Pollena primary deposits are completely lacking and only the syn-eruptive lahar deposits are present on top of the late Roman paleosol. Where preserved, the paleosol often has an undulated surface due to cultivation (plowing and hoeing). The Pollena eruption sequence consists of an alternation of coarse pumice and fine ash layers emplaced by fallout (*a* in Fig. C8). It is up to 50 cm thick and ends with a cohesive yellowish ash layer (*b* in Fig. C8), overlain by the lahar deposits, generally composed of two to three flow units (*c* in Fig. C8). The total thickness of the lahars is largely variable with maxima at the base of the slopes where it can reach 2–3 m. In some excavations we did not reach the base of the deposit, which is deeper than 3.5 m. In Fig. C8, it is possible to observe a complete sequence of the Pollena deposits overlying a late Roman paleosol. The sequence includes fallout layers and thick lahar deposits. The latter are always massive and matrix-supported and contain abundant scattered pumice and lithic fragments (lithofacies Gms). In some cases, the lower part contains several limestone fragments up to 10 cm in diameter. The described deposit has been also found in the Roman amphitheater of Avella, where it has a variable thickness (order of decimetric). Here, it has been almost completely excavated and only remnants are presently exposed.

Generally, the upper part of the sequences is composed of an alternation of plane-parallel to cross-layered sands and gravels, with abundant rounded limestone fragments, emplaced by several alluvial episodes (post-eruptive) (lithofacies Sh-Ss). In these post-eruptive deposits, it is not uncommon to find terracotta fragments from the Imperial Roman age.

The Pollena primary and secondary sequences are overlain by a mature paleosol with frequent evidence of cultivation (plowing, *p* in Fig. C9) and locally by the 1631 eruption deposits. The primary deposit related to the 1631 eruption is not always present. It is an up to 2 cm (*a* in Fig. C9) thick ash layer, gray-violet in color, deposited by fallout deposit and overlaying a plowed paleosol (p in Fig. C9). It is overlain by lahar deposits (*b* in Fig. C9) composed of several units and characterized by contrasting grain sizes. The deposits are composed of medium ash, are massive and

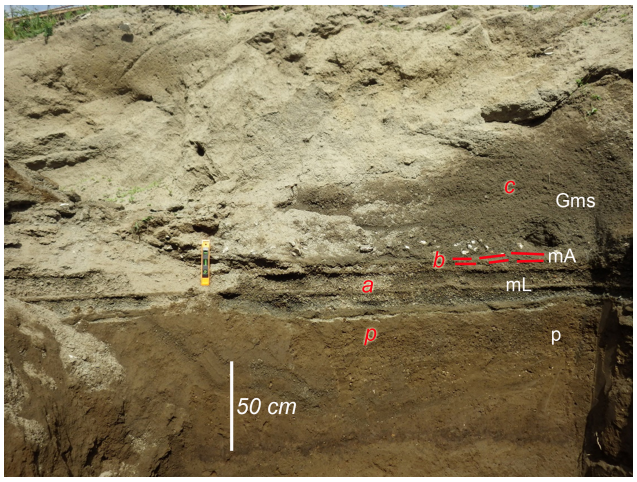

Figure C8. Avella–Baiano Valley; the Pollena primary deposit (a, b) lies on plowed soil (p) and is covered by at least three flow units of lahars (c). For the description of lithofacies see Table 2.

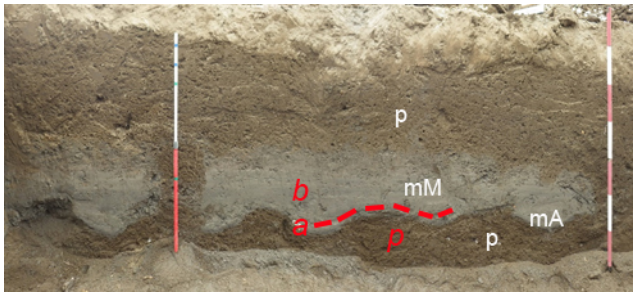

Figure C9. Avella–Baiano Valley, in particular the 1631 primary (a) and secondary deposits (b, syn-eruptive lahars) in a trench at the Cicciano locality. For the description of lithofacies see Table 2.

matrix-supported, and contain abundant scattered millimeter- to centimeter-sized pumice fragments (all with the same lithology of the primary deposits) and sometimes vegetal remain traces (lithofacies Gms).

C5 Area 5 – Lauro Valley

Lauro Valley has characteristics similar to the Avella–Baiano Valley, but the primary deposits of Pollena and 1631 eruptions are thicker (Figs. 5 and 6) and coarser. In this valley, the sequences are also locally deeply eroded. In fact, the deposits of the Pollena eruption (normally 50–70 cm thick) (Fig. C10) are sometimes missing. They overlie a mature paleosol with abundant traces of cultivation. Overall, the characteristics of the deposits are very similar to the ones of the Nola area (10–15 km from Apennine source valleys). The overlying lahar deposits are always massive, matrix-supported, and composed of fine and very cohesive ash with abundant scattered pumices and lithic fragments (similar in lithology to those of the primary deposits) (lithofacies Gms). These deposits have a highly variable thickness, with a measured maximum of

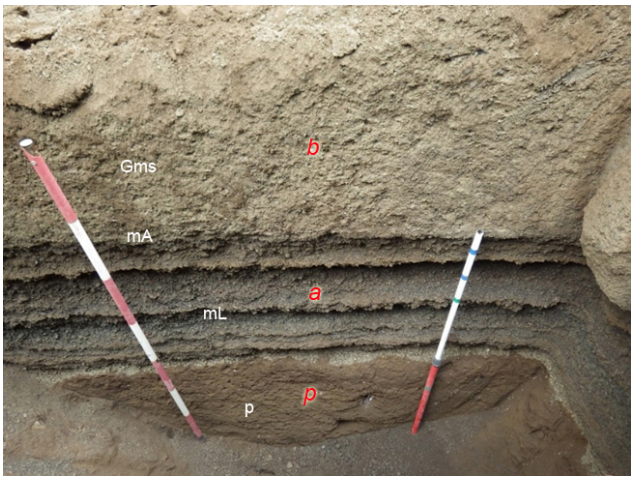

Figure C10. Lauro Valley, Pago del Vallo. In particular, a indicates the sequence of the Pollena fallout deposits overlain by syn-eruptive lahars (b), and p indicates late Roman paleosol at the base. For the description of lithofacies see Table 2.

Figure C11. Taurano (Villa Lauro); baulk showing a thick sequence of the Pollena syn-eruptive lahar units filling the Roman villa. Some units engulf and transport pieces of walls and large blocks. The fallout sequence is not exposed in the villa, likely due to the presence of a roof. The deposit below the damaged walls is composed of multiple lahar units represented by the Gms lithofacies (see Table 2).

2 m, but are sometimes reduced by erosion. In some trenches the base of the sequences was deeper than the investigated depth (> 3.5 m).

It is possible to evaluate the effects of the lahars on building in the Roman Villa di Lauro, at Taurano, where a 70 cm thick fallout is overlain, without paleosol, by syn-eruptive lahars which engulfed and transported pieces of walls, bricks, and potteries. The lahar deposits are matrix-supported, are composed of fine to coarse ash, and contain abundant pumice lapilli (all similar to the Pollena fallout deposits). They are

massive and cohesive and have a thickness up to about 1 m, thickening in depressions and near barriers (Fig. C11).

The sequence related to the eruption of 1631 is not always present, but it is possible to find its primary deposit, composed of a basal layer of stratified fine and medium thin ash beds and minor dark pumice and lithic fragments overlain by a thin, very fine and cohesive accretionary lapilli-rich ash bed. The maximum measured thickness is 30 cm. The overlying lahar deposits are massive and matrix-supported, composed of fine to coarse ash, and contain abundant pumice fragments of the primary deposit.

Data availability. Data are publicly available at this online repository: https://doi.org/10.5281/zenodo.10814860 (Di Vito et al., 2024).

Author contributions. MADV: conceptualization, investigation, methodology, writing (original draft preparation, review and editing), funding acquisition; IR: data curation, investigation, writing (original draft preparation); SdV: investigation, writing (original draft preparation, review and editing); DMD: investigation, methodology, data curation, writing (original draft preparation, review and editing); MB: data curation, methodology, writing (original draft preparation); MdMV: writing (review and editing); MR: conceptualization, writing (review and editing); LS: writing (review and editing); GZ: investigation, writing (review and editing); EZ: investigation, methodology, writing (original draft preparation); AC: conceptualization, writing (review and editing), funding acquisition.

Competing interests. The contact author has declared that none of the authors has any competing interests.

Disclaimer. The paper does not necessarily represent DPC official opinion and policies.

Publisher's note: Copernicus Publications remains neutral with regard to jurisdictional claims made in the text, published maps, institutional affiliations, or any other geographical representation in this paper. While Copernicus Publications makes every effort to include appropriate place names, the final responsibility lies with the authors.

Acknowledgements. This work benefited from the agreement between Istituto Nazionale di Geofisica e Vulcanologia and the Italian Presidenza del Consiglio dei Ministri, Dipartimento della Protezione Civile (DPC), Convenzione INGV-DPC All B2. The work was also supported by the INGV project Pianeta Dinamico – Working Earth – Task V3 (MDV). We thank Ulrich Kueppers, Lucia Capra, an anonymous reviewer, and the editor Andrea Di Muro very much for their help in improving this paper in the revision process.

Financial support. This research has been supported by the Dipartimento della Protezione Civile, Presidenza del Consiglio dei Ministri (grant no. D54I19000280001 (DPC-INGV B2 2019–2021)). The work was also supported by the INGV project Pianeta Dinamico – Working Earth (grant no. D53J19000170001 (Pianeta Dinamico) – "Fondo finalizzato al rilancio degli investimenti delle amministrazioni centrali dello Stato e allo sviluppo del Paese", legge 145/2018) – Task V3 (MDV).

Review statement. This paper was edited by Andrea Di Muro and reviewed by Ulrich Kueppers, Lucia Capra, and one anonymous referee.

References

Acocella, V. and Funiciello, R.: Transverse systems along the extensional Tyrrhenian margin of Central Italy and their influence on volcanism, Tectonics, 25, 1–24, https://doi.org/10.1029/2005TC001845, 2006.

Arguden, A. T. and Rodolfo, K. S.: Sedimentologic and dynamic differences between hot and cold laharic debris flows of Mayon Volcano, Philippines, Geol. Soc. Am. Bull., 102, 865–876, 1990.

Bardot, L.: Emplacement temperature determinations of proximal pyroclastic deposits on Santorini, Greece, and their implications, B. Volcanol., 61, 450–467, https://doi.org/10.1007/PL00008911, 2000.

Bardot, L. and McClelland, E.: The reliability of emplacement temperature estimates using paleomagnetic methods: a case study from Santorini, Greece, Geophys. J. Int., 143, 39–51, https://doi.org/10.1046/j.1365-246x.2000.00186.x, 2000.

Bartole, R.: Tectonic Structure of the Latian-Campanian Shelf (Tyrrhenian Sea), Bollettino di Oceanologia Teorica Applicata, 2, 197–230, 1984.

Baumann, V., Bonadonna, C., Cuomo, S., and Moscariello, M.: Modelling of erosion processes associated with rainfall-triggered lahars following the 2011 Cordon Caulle eruption (Chile), J. Volcanol. Geoth. Res., 390, 106727, https://doi.org/10.1016/j.jvolgeores.2019.106727, 2020.

Bisson, M., Pareschi, M. T., Zanchetta, G., Sulpizio, R., and Santacroce, R.: Volcaniclastic debris-flow occurrences in the Campania region (Southern Italy) and their relation to Holocene–Late Pleistocene pyroclastic fall deposits: implications for large-scale hazard mapping, B. Volcanol., 70, 157–167, https://doi.org/10.1007/s00445-007-0127-4, 2007.

Bisson, M., Zanchetta, G., Sulpizio, R., and Demi, F.: A map for volcaniclastic debris flow hazards in Apennine areas surrounding the Vesuvius volcano (Italy), J. Maps, 9, 230–238, https://doi.org/10.1080/17445647.2013.768948, 2013.

Bisson, M., Spinetti, C., and Sulpizio, R.: Volcaniclastic flow hazard zonation in the Sub-Apennine Vesuvian area using GIS and remote sensing, Geosphere, 10, 1419–1431, https://doi.org/10.1130/GES01041.1, 2014.

Blott, S.J., and Pye, K.: Gradistat: A Grain Size Distribution and Statistics Package for the Analysis of Unconsolidated Sediments, Earth Surf. Proc. Land., 26, 1237–1248, https://doi.org/10.1002/esp.261, 2001.

Braccini, G. C.: Dell'Incendio Fattosi nel Vesuvio a XVI di Dicembre MDCXXXI, Secondino Roncagliolo, 104 pp., https://play.google.com/store/books/details/Giulio_Cesare_Braccini_Dell_incendio_fattosi_nel_V?id=1aBxWGZR6TMC&gl=US (last access: 10 January 2024), 1632.

Brancaccio, L., Cinque, A., Romano, P., Rosskopf, C., Russo, F., Santangelo, N., and Santo, A.: Geomorphology and neotectonic evolution of a sector of the Tyrrhenian flank of the Southern Apennines (Region of Naples, Italy), Zeit. Geomorph. N. F. Suppl.-Bd., 82, 47–58, 1991.

Breard, E. C. P. and Lube, G.: Inside pyroclastic density currents – uncovering the enigmatic flow structure and transport behaviour in large-scale experiments, Earth Planet. Sc. Lett., 458, 22–36, https://doi.org/10.1016/j.epsl.2016.10.016, 2017.

Breard, E. C. P., Lube, G., Cronin, S. J., and Valentine, G. A.: Transport and deposition processes of the hydrothermal blast of the 6 August 2012 Te Maari eruption, Mt. Tongariro, B. Volcanol., 77, 100, https://doi.org/10.1007/s00445-015-0980-5, 2015.

Brocchini, D., Principe, C., Castradori, D., Laurenzi, M. A., and Gorla, L.: Quaternary evolution of the southern sector of the Campanian Plain and early Somma-Vesuvius activity: insights from the Trecase 1 well, Miner. Petrol., 73, 67–91, https://doi.org/10.1007/s007100170011, 2001.

Capra, L., Sulpizio, R., Marquez-Ramirez, V. H., Coviello, V., Doronzo, D. M., Arambula-Mendoza, R., and Cruz, S.: The anatomy of a pyroclastic density current: the 10 July 2015 event at Volcan de Colima (Mexico), B. Volcanol., 80, 34, https://doi.org/10.1007/s00445-018-1206-4, 2018.

Carling, P. A.: Freshwater megaflood sedimentation: What can we learn about generic processes?, Earth-Sci. Rev., 125, 87–113, https://doi.org/10.1016/j.earscirev.2013.06.002, 2013.

Carrara, E., Iacobucci, F., Pinna, E., and Rapolla, A.: Gravity and magnetic survey of the Campanian volcanic area, S. Italy, Boll. Geof. Teor. Appl., 15, 39–51, 1973.

Cas, R. A. F., Wright, H. M. N., Folkes, C. B., Lesti, C., Porreca, M., Giordano, G., and Viramonte, J. G.: The flow dynamics of an extremely large volume pyroclastic flow, the 2.08-Ma Cerro Galán Ignimbrite, NW Argentina, and comparison with other flow types, B. Volcanol., 73, 1583–1609, https://doi.org/10.1007/s00445-011-0564-y, 2011.

Cinque, A. and Robustelli, G.: Alluvial and coastal hazards caused by long-range effects of Plinian eruptions: The case of the Lattari Mts. After the AD 79 eruption of Vesuvius, Geol. Soc. Lond. Spec. Publ., 322, 155–171, https://doi.org/10.1144/SP322.7, 2009.

Cioni, R., Santacroce, R., and Sbrana, A.: Pyroclastic deposits as a guide for reconstructing the multi-stage evolution of the Somma-Vesuvius Caldera, B. Volcanol., 60, 207–222, 1999.

Cioni, R., Gurioli, L., Lanza, R., and Zanella, E.: Temperatures of A.D. 79 pyroclastic density current deposits (Vesuvius, Italy), J. Geophys. Res., 109, B02207, https://doi.org/10.1029/2002JB002251, 2004.

Costa, J. E.: Hydraulic modeling for lahar hazards at Cascades volcanoes, Environmental Engineering Geoscience, 3, 21–30, https://doi.org/10.2113/gseegeosci.III.1.21, 1997.

D'Argenio, B., Pescatore, T. S., and Scandone, P.: Schema geologico dell'Appennino meridionale (Campania e Lucania), In: Moderne vedute sulla geologia dell'Appennino. Convegno (Roma, 16–18 Febbraio 1972), Accademia Nazionale dei Lincei, Problemi Attuali di Scienza e Cultura, Quaderni 183, 49–72, https://www.pconti.net/Scandone-Web/DArgenio1973.pdf (last access: 10 January 2024), 1973.

de' Michieli Vitturi, M., Costa, A., Di Vito, M. A., Sandri, L., and Doronzo, D. M.: Lahar events in the last 2000 years from Vesuvius eruptions – Part 2: Formulation and validation of a computational model based on a shallow layer approach, Solid Earth, 15, 437–458, https://doi.org/10.5194/se-15-437-2024, 2024.

De Simone, G. F., Perrotta, A., and Scarpati, C.: L'eruzione del 472 d.C. ed il suo impatto su alcuni siti alle falde del Vesuvio, Rivista Studi Pompeiani, 22, 61–71, http://www.jstor.org/stable/44291260 (last access: 10 January 2024), 2011.

De Vivo, B., Rolandi, G., Gans, P. B., Calvert, A., Bohrson, W. A., Spera, F. J., and Belkin, H. E.: New constraints on the pyroclastic eruptive history of the Campanian volcanic Plain (Italy), Miner. Petrol., 73, 47–65, https://doi.org/10.1007/s007100170010, 2001.

Di Crescenzo, G. and Santo, A.: Nuovo contributo sul ruolo svolto dai livelli pomicei nelle aree di distacco delle frane di colata rapida dei massicci carbonatici campani, Convegno Nazionale La mitigazione del rischio da colate di fango a Sarno e negli altri Comuni colpiti dagli eventi del maggio 1998. Napoli, 2 e 3 maggio 2005–Sarno 4 e 5 maggio 2005, https://www.researchgate.net/publication/258515737_Nuovo_contributo_sul_ruolo_svolto_dai_livelli_pomicei_nelle_aree_di_distacco_delle_frane_di_colata_rapida_dei_massicci_carbonatici_campani (last access: 10 January 2024), 2005.

Di Vito, M. A., Sulpizio, R., and Zanchetta, G.: I depositi ghiaiosi della valle dei torrenti Clanio e Acqualonga (Campania centro-orientale): significato stratigrafico e ricostruzione paleoambientale, Il Quaternario Italian Journal of Quaternary Sciences, 11, 273–286, 1998.

Di Vito, M. A., Zanella, E., Gurioli, L., Lanza, R., Sulpizio, R., Bishop, J., Tema, E., Boenzi, G., and Laforgia, E.: The Afragola settlement near Vesuvius, Italy: The destruction and abandonment of a Bronze Age village revealed by archeology, volcanology and rock-magnetism, Earth Planet. Sc. Lett., 277, 408–421, https://doi.org/10.1016/j.epsl.2008.11.006, 2009.

Di Vito, M. A., Castaldo, N., de Vita, S., Bishop, J., and Vecchio, G.: Human colonization and volcanic activity in the eastern Campania Plain (Italy) between the Eneolithic and Late Roman periods, Quatern. Int., 303, 132–141, https://doi.org/10.1016/j.quaint.2013.01.001, 2013.

Di Vito, M. A., Calcaterra, D., Petrosino, P., Zanchetta, G., de Vita, S., Marotta, E., Cesarano, M., De Simone, A., Sansivero, F., and Rucco, I.: Landslides, volcanism and volcano-tectonics: the fragility of the Neapolitan territory, Geological Field Trips and Maps, 11, 1–53, https://doi.org/10.3301/GFT.2019.01, 2019a.

Di Vito, M. A., Talamo, P., de Vita, S., Rucco, I., Zanchetta, G., and Cesarano, M.: Dynamics and effects of the Vesuvius Pomici di Avellino Plinian eruption and related phenomena on the Bronze Age landscape of Campania region (Southern Italy), Quatern. Int., 499, 231–244, https://doi.org/10.1016/j.quaint.2018.03.021, 2019b.

Di Vito, M. A., Rucco, I., de Vita, S., Doronzo, D. M., Bisson, M., and Zanella, E.: Field data collected from pyroclastic and lahar deposits of the 472 AD (Pollena) and 1631 Vesuvius eruptions, Zenodo [data set], https://doi.org/10.5281/zenodo.10814860, 2024.

Doronzo, D. M.: Two new end members of pyroclastic density currents: Forced-convection dominated and inertia-dominated, J. Volcanol. Geoth. Res., 219–220, 87–91, https://doi.org/10.1016/j.jvolgeores.2012.01.010, 2012.

Doronzo, D. M.: Aeromechanic analysis of pyroclastic density currents past a building, B. Volcanol., 75, 684, https://doi.org/10.1007/s00445-012-0684-z, 2013.

Doronzo, D. M. and Dellino, P.: Hydraulics of subaqueous ash flows as deduced from their deposits: 2. Water entrainment, sedimentation, and deposition, with implications on pyroclastic density current deposit emplacement, J. Volcanol. Geoth. Res., 258, 176–186, https://doi.org/10.1016/j.jvolgeores.2013.04.013, 2013.

Doronzo, D. M., Martí, J., Sulpizio, R., and Dellino, P.: Aerodynamics of stratovolcanoes during multiphase processes, J. Geophys. Res., 117, B01207, https://doi.org/10.1029/2011JB008769, 2012.

Duller, R. A., Mountney, N. P., Russell, A. J., and Cassidy, N. C.: Architectural analysis of a volcaniclastic jökulhlaup deposit, southern Iceland: sedimentary evidence for supercritical flow, Sedimentology, 55, 939–964, https://doi.org/10.1111/j.1365-3091.2007.00931.x, 2008.

Faccenna, C., Funiciello, R., Bruni, A., Mattei, M., and Sagnotti, L.: Evolution of a transfer related basin: the Ardea basin (Latium, Central Italy), Basin Res., 6, 35–46, https://doi.org/10.1111/j.1365-2117.1994.tb00073.x, 1994.

Fedi, M. and Rapolla, A.: The Campanian Volcanic Area: analysis of the magnetic and gravimetric anomalies, Boll. Soc. Geol. Ital., 106, 793–805, 1987.

Finetti, I. and Morelli, C.: Esplorazione di sismica a riflessione nei Golfi di Napoli e Pozzuoli, B. Geofis. Teor. Appl., 16, 175–222, 1974.

Fiorillo, F. and Wilson, R. C.: Rainfall induced debris flows in pyroclastic deposits, Campania (southern Italy), Eng. Geol., 75, 263–289, https://doi.org/10.1016/j.enggeo.2004.06.014, 2004.

Giordano, G., Zanella, E., Trolese, M., Baffioni, C., Vona, A., Caricchi, C., De Benedetti, A. A., Corrado, S., Romano, C., Sulpizio, R., and Geshi, N.: Thermal interactions of the AD79 Vesuvius pyroclastic density currents and their deposits at Villa dei Papiri (Herculaneum archaeological site, Italy), Earth Planet. Sc. Lett., 490, 180–192, https://doi.org/10.1016/j.epsl.2018.03.023, 2018.

Girolami, L., Roche, O., Druitt, T., and Corpetti, T.: Velocity fields and depositional processes in laboratory ash flows, with implications for the dynamics of dense pyroclastic flows, B. Volcanol., 72, 747–759, https://doi.org/10.1007/s00445-010-0356-9, 2010.

Gurioli, L., Pareschi, M. T., Zanella, E., Lanza, R., Deluca, E., and Bisson, M.: Interaction of pyroclastic density currents with human settlements: Evidence from ancient Pompeii, Geology, 33, 441–444, https://doi.org/10.1130/G21294.1, 2005.

Gurioli, L., Sulpizio, R., Cioni, R., Sbrana, A., Santacroce, R., Luperini, W., and Andronico, D.: Pyroclastic flow hazard assessment at Somma-Vesuvius based on the geological record, B. Volcanol., 72, 1021–1038, https://doi.org/10.1007/s00445-010-0379-2, 2010.

Guzman, S., Doronzo, D. M., Martí, J., and Seggiaro, R.: Characteristics and emplacement mechanisms of the Coranzulí ignimbrites (Central Andes), Sediment. Geol., 405, 105699, https://doi.org/10.1016/j.sedgeo.2020.105699, 2020.

Ippolito, F., Ortolani, F., and Russo, M.: Struttura marginale tirrenica dell'Appennino campano: reinterpretazioni di dati di antiche ricerche di idrocarburi, Mem. Soc. Geol. Ital., 12, 227–250, 1973.

Iverson, R. M., Denlinger, R. P., LaHusen, R. G., and Logan, M.: Two-phase debris-flow across 3-D terrain: model predictions and experimental tests, in: Debris-Flow Hazard Mitigation, Mechanics, Prediction, and Assessment, edited by: Wieczorek, G. F. and Naeser, N. D., Taipei, Taiwan, 16–18 August 2000, Rotterdam, Balkema, 521–529, ISBN 978 90 5966 059 5, 2000.

Jenkins, S. F., Phillips, J. C., Price, R., Feloy, K., Baxter, P. J., Sri Hadmoko, D., and de Bélizal, E.: Developing building-damage scales for lahars: application to Merapi volcano Indonesia, B. Volcanol., 77, 1–17, https://doi.org/10.1007/s00445-015-0961-8, 2015.

Lesti, C., Porreca, M., Giordano, G., Mattei, M., Cas, R., Wright, H., and Viramonté, J. G.: High temperature emplacement of the Cerro Galán and Toconquis Group ignimbrites (Puna plateau, NW Argentina) determined by TRM analyses, B. Volcanol., 73, 1535–1565, https://doi.org/10.1007/s00445-011-0536-2, 2011.

Lowe, D. R.: Suspended-load fallout rate as an independent variable in the analysis of current structures, Sedimentology, 35, 765–776, https://doi.org/10.1111/j.1365-3091.1988.tb01250.x, 1988.

Lowe, D. R., Williams, S. N., Leigh, H., Connort, C. B., Gemmell, J. B., and Stoiber, R. E.: Lahars initiated by the 13 November 1985 eruption of Nevado del Ruiz, Colombia, Nature, 324, 51–53, https://doi.org/10.1038/324051a0, 1986.

Lube, G., Cronin, S., Manville, V., Procter, J., Cole, S., and Freundt, A.: Energy growth in laharic mass flows, Geology, 40, 475–478, https://doi.org/10.1130/G32818.1, 2012.

Macedonio, G. and Pareschi, M. T.: Numerical simulation of some lahars from Mount St. Helens, J, Volcanol. Geoth. Res., 54, 65–80, https://doi.org/10.1016/0377-0273(92)90115-T, 1992.

Mariani, M. and Prato, R.: I bacini neogenici costieri del margine tirrenico: approccio sismico-stratigrafico, Mem. Soc. Geol. Ital., 41, 519–531, 1988.

Marotta, E., Berrino, G., de Vita, S., Di Vito, M. A., and Camacho, A. G.: Structural setting of the Ischia resurgent caldera (Southern Tyrrhenian Sea, Italy) by integrated 3D gravity inversion and geological models, in: Volcanic Island: from Hazard Assessment to Risk Mitigation, edited by: Marotta, E., D'Auria, L., Zaniboni, F. and Nave, R., Geological Society, London, Special Publications, 519, 29–46, https://doi.org/10.1144/sp519-2022-129, 2022.

Martí, J., Doronzo, D. M., Pedrazzi, D., and Colombo, F.: Topographical controls on small-volume pyroclastic flows, Sedimentology, 66, 2297–2317, https://doi.org/10.1111/sed.12600, 2019.

McClelland, E.: Theory of CRM acquired by grain growth, and its implications for TRM discrimination and paleointensity determination in igneous rocks, Geophys. J. Int., 126, 271–280, https://doi.org/10.1111/j.1365-246X.1996.tb05285.x, 1996.

McClelland, E. and Druitt, T. H.: Paleomagnetic estimates of emplacement temperatures of pyroclastic deposits on Santorini, Greece, B. Volcanol., 51, 16–27, https://doi.org/10.1007/BF01086758, 1989.

Newhall, C. G. and Punongbayan, R. (Eds.): Fire and mud: eruptions and lahars of Mount Pinatubo, Philippines, Quezon City: Philippine Institute of Volcanology and Seismology, 1126 pp., https://pubs.usgs.gov/pinatubo/ (last access: 10 January 2024), 1996.

Orsi, G., de Vita, S., and Di Vito, M.A.: The restless, resurgent Campi Flegrei Nested Caldera Italy.: constraints on its evolu-

tion and configuration, J. Volcanol. Geoth. Res., 74, 179–214, https://doi.org/10.1016/S0377-0273(96)00063-7, 1996.

Pareschi, M. T., Favalli, M., Giannini, F., Sulpizio, R., Zanchetta, G., and Santacroce, R.: May 5, 1998, Debris flows in circumvesuvian areas (Southern Italy), insights for hazard assessment, Geology, 28, 639–642, https://doi.org/10.1130/0091-7613(2000)28<639:MDFICA>2.0.CO;2, 2000.

Pareschi, M. T., Santacroce, R., Sulpizio, R., and Zanchetta, G.: Volcaniclastic debris flows in the Clanio Valley (Campania, Italy): Insights for the assessment of hazard potential, Geomorphology, 43, 219–231, https://doi.org/10.1016/S0169-555X(01)00134-9, 2002.

Patacca, E. and Scandone, P.: Geology of the Southern Apennines, Bollettino della Società Geologica Italiana Special Issue 7, 75–119, https://www.researchgate.net/publication/267507693_Geology_of_the_Southern_Apennines (last access: 10 January 2024), 2007.

Paterson, G. A., Roberts, A. P., Mac Niocaill, C., Muxworthy, A. R., Gurioli, L., Viramonté, J. G., Navarro, C., and Weider, S.: Paleomagnetic determination of emplacement temperatures of pyroclastic deposits: un under-utilized tool, B. Volcanol., 72, 309–330, https://doi.org/10.1007/s00445-009-0324-4, 2010.

Peccerillo, A.: Plio-Quaternary magmatism in Italy, Episodes, 26, 222-226, https://doi.org/10.18814/epiiugs/2003/v26i3/012, 2003.

Perrotta, A., Scarpati, C., Luongo, G., and Aoyagi, M.: Burial of Emperor Augustus' villa at Somma Vesuviana (Italy) by post-79 AD Vesuvius eruptions and reworked (lahars and stream flow) deposits, J. Volcanol. Geoth. Res., 158, 445–466, https://doi.org/10.1016/j.jvolgeores.2006.08.006, 2006.

Pierson, T. C.: Initiation and flow behavior of the 1980 Pine Creek and Muddy River lahars, Mt. St. Helens, Washington, Geol. Soc. Am. Bull., 96, 1056-1069, https://doi.org/10.1130/0016-7606(1985)96<1056:IAFBOT>2.0.CO;2, 1985.

Piochi, M., Pappalardo, L., and De Astis, G.: Geo-chemical and isotopical variations within the Campanian Comagmatic Province: implications on magma source composition, Ann. Geophys.-Italy, 47, 1485–1499, https://doi.org/10.4401/ag-8757, 2004.

Pittari, A., Cas, R. A. F., Monaghan, J. J., and Martí, J.: Instantaneous dynamic pressure effects on the behaviour of lithic boulders in pyroclastic flows: the Abrigo Ignimbrite, Tenerife, Canary Island, B. Volcanol., 69, 265–279, https://doi.org/10.1007/s00445-006-0072-7, 2007.

Porreca, M., Mattei, M., Mac Niocaill, C., Giordano, G., McClelland, E., and Funiciello, R.: Paleomagnetic evidence for low-temperature emplacement of the phreatomagmatic Peperino Albano ignimbrite (Colli Albani volcano, Central Italy), B. Volcanol., 70, 877–893, https://doi.org/10.1007/s00445-007-0176-8, 2007.

Roche, O.: Depositional processes and gas pore pressure in pyroclastic flows: an experimental perspective, B. Volcanol., 74, 1807–1820, https://doi.org/10.1007/s00445-012-0639-4, 2012.

Roche, O.: Nature and velocity of pyroclastic density currents inferred from models of entrainment of substrate lithic clasts, Earth Planet. Sc. Lett., 418, 115–125, https://doi.org/10.1016/j.epsl.2015.03.001, 2015.

Roche, O., Niño, Y., Mangeney, A., Brand, B., Pollock, N., and Valentine, G. A.: Dynamic pore-pressure variations induce substrate erosion by pyroclastic flows, Geology, 41, 1107–1110, https://doi.org/10.1130/G34668.1, 2013.

Rodolfo, K. S.: The hazard from lahars and jökulhlaups, in: Encyclopedia of Volcanoes, edited by: Sigurdssson, H., Houghton, B., McNutt, S., Rymer, H., and Stix, J., Academic Press, London, 973–995, ISBN 9780080547985, 2000.

Rodolfo, K. S. and Arguden, A. T.: Rain-lahar generation and sediment-delivery systems at Mayon Volcano, Philippines, in: Sedimentation in Volcanic Settings, SEPM Special Publication, 45, edited by: Fisher, R. V. and Smith, G. A., 71–88, https://doi.org/10.2110/pec.91.45.0071, 1991.

Rodríguez-Sedano, L. A., Sarocchi, D., Caballero, L., Borselli, L., Ortiz-Rodríguez, A. J., Cerca-Ruiz, M. F., Moreno-Chávez, G., and Franco Ramos, O.: Post-eruptive lahars related to the 1913 eruption in La Lumbre Ravine, Volcán de Colima, Mexico: The influence of ravine morphometry on flow dynamics, J. Volcanol. Geoth. Res., 421, 107423, https://doi.org/10.1016/j.jvolgeores.2021.107423, 2022.

Rolandi, G., Barrella, A. M., and Borrelli, A.: The 1631 eruption of Vesuvius, J. Volcanol. Geoth. Res., 58, 183–201, https://doi.org/10.1016/0377-0273(93)90107-3, 1993.

Rolandi, G., Munno, R., and Postiglione, I.: The A.D. 472 eruption of the Somma volcano, J. Volcanol. Geoth. Res., 129, 291–319, https://doi.org/10.1016/S0377-0273(03)00279-8, 2004.

Rosi, M. and Santacroce, R.: The A.D. 472 "Pollena" eruption: volcanological and petrological data for this poorly-known, Plinian-type event at Vesuvius, J. Volcanol. Geoth. Res., 17, 249–271, https://doi.org/10.1016/0377-0273(83)90071-9, 1983.

Rosi, M., Principe, C., and Vecci, R.: The 1631 Vesuvius eruption. A reconstruction based on historical and stratigraphical data, J. Volcanol. Geoth. Res., 58, 151–182, https://doi.org/10.1016/0377-0273(93)90106-2, 1993.

Russell, A. J. and Knudsen, O.: An ice-contact rhythmite (turbidite) succession deposited during the November 1996 catastrophic outburst flood (jökulhlaup), Skeidarárjökull, Iceland, Sediment. Geol., 127, 1–10, https://doi.org/10.1016/S0037-0738(99)00024-X, 1999.

Sandri, L., de' Michieli Vitturi, M., Costa, A., Di Vito, M. A., Rucco, I., Doronzo, D. M., Bisson, M., Gianardi, R., de Vita, S., and Sulpizio, R.: Lahar events in the last 2000 years from Vesuvius eruptions – Part 3: Hazard assessment over the Campanian Plain, Solid Earth, 15, 459–476, https://doi.org/10.5194/se-15-459-2024, 2024.

Santacroce, R., Sbrana, A., Andronico, D., Cioni, R., Di Vito, M., Marianelli, P., Sulpizio, R., Zanchetta, G., Arrighi, S., Benvenuti, E., Gurioli, L., Leoni, F. M., and Luperini, W.: Carta Geologica del Vesuvio in scala 1 : 15.000, in: Cartografia derivata dai rilievi geologici in scala 1 : 10.000 Regione Campania e dai rilievi in scala 1 : 25.000 del Progetto CARG, edited by: Santacroce, R. and Sbrana A., S.EL.C.A., Firenze, https://repositories.dst.unipi.it/index.php/carte/item/124-carta-geologica-del-vesuvio (last access: 10 January 2024), 2003.

Santacroce, R., Cioni, R., Marianelli, P., Sbrana, A., Sulpizio, R., Zanchetta, G., Donahue, D.J., and Joron, J. L.: Age and whole rock-glass compositions of proximal pyroclastics from the major explosive eruptions of Somma-Vesuvius: A review as a tool for distal tephrostratigraphy, J. Volcanol. Geoth. Res., 177, 1–18, https://doi.org/10.1016/j.jvolgeores.2008.06.009, 2008.

Santangelo, N., Romano, P., Ascione, A., and Russo Ermolli, E.: Quaternary evolution of the Southern Apennines coastal plains: A review, Geol. Carpath., 68, 43–56, https://doi.org/10.1515/geoca-2017-0004, 2017.

Scott, K. M.: Magnitude and frequency of lahars and lahar-runout flows in the Toutle-Cowlitz River System, U. S. Geological Survey Professional Paper 1447-B, 1–33, https://pubs.usgs.gov/pp/1447b/report.pdf (last access: 10 January 2024), 1989.

Scott, K. M., Vallance, J. W., and Pringle, P. T.: Sedimentology, behavior, and hazard of debris flows at Mount Rainer, Washington, U. S. Geological Survey Professional Paper 1547, 1–56, https://doi.org/10.3133/pp1547, 1995.

Scott, K. M., Macìas, J. L., Naranjo, J. A., Rodriguez, S., and McGeehin, J. P.: Catastrophic debris flows transformed from landslide in volcanic terrains: mobility, hazard assessment and mitigation strategies, U. S. Geological Survey Professional Paper 1630, 1–59, https://doi.org/10.3133/pp1630, 2001.

Sheridan, M. F., Bonnard, C., Carrero, C., Siebe, C., Strauch, W., Navarro, M., Calero, J. C., and Trujillo, N. B.: Report of the 30 October 1998 rock fall/avalanche and breakout flow of Casita Volcano, Nicaragua, triggered by Hurracane Mitch, Landslide News, 12, 2–4, 1999.

Siebe, C., Schaaf, P., and Urrutia-Fucugauchi, J.: Mammoth bones embedded in a late Pleistocene lahar from Popocatépetl volcano, near Tocuila, central Mexico, Geol. Soc. Am. Bull., 111, 1550–1567, https://doi.org/10.1130/0016-7606(1999)111<1550:MBEIAL>2.3.CO;2, 1999.

Smith, G., Williams, R., Rowley, P. J., and Parsons, D. R.: Investigation of variable aeration of monodisperse mixtures: implications for pyroclastic density currents, B. Volcanol., 80, 67, https://doi.org/10.1007/s00445-018-1241-1, 2018.

Spence, R. J. S., Zuccaro, G., Petrazzuoli, S., and Baxter, P. J.: Resistance of buildings to pyroclastic flows: analytical and experimental studies and their application to Vesuvius, Nat. Hazards Rev., 5, 48–59, https://doi.org/10.1061/(ASCE)1527-6988(2004)5:1(48), 2004.

Stanzione, M., Di Vito, M. A., Aurino, P., and Lumaga, M. R. B.: Sacred plant impressions from Somma-Vesuvius volcanic ash deposits: A medicinal garden in Late Antique Acerra (Naples, Campania, Italy)?, J. Archaeol. Sci., 47, 103802, https://doi.org/10.1016/j.jasrep.2022.103802, 2023.

Sulpizio, R., Mele, D., Dellino, P., and La Volpe, L.: A complex, Subplinian-type eruption from low-viscosity, phonolitic to tephri-phonolitic magma: the AD 472 (Pollena) eruption of Somma-Vesuvius, Italy, B. Volcanol., 67, 743–767, https://doi.org/10.1007/s00445-005-0414-x, 2005.

Sulpizio, R., Zanchetta, G., Demi, F., Di Vito, M. A., Pareschi, M. T., and Santacroce, R.: The Holocene syneruptive volcaniclastic debris flows in the Vesuvian area: Geological data as a guide for hazard assessment, Geol. S. Am. S., 402, 203–221, https://doi.org/10.1130/2006.2402(10), 2006.

Sulpizio, R., Dellino, P., Doronzo, D. M., and Sarocchi, D.: Pyroclastic density currents: state of the art and perspectives, J. Volcanol. Geoth. Res., 283, 36–65, https://doi.org/10.1016/j.jvolgeores.2014.06.014, 2014.

Stanzione, M., Di Vito, M. A., Aurino, P., and Barone Lumaga, M. R.: Sacred plant impressions from Somma-Vesuvius volcanic ash deposits: A medicinal garden in Late Antique Acerra (Naples, Campania, Italy)?, J. Archaeol. Sci., 47, 103802, https://doi.org/10.1016/j.jasrep.2022.103802, 2023.

Tema, E., Zanella, E., Pavón-Carrasco, F. J., Kondopoulou, D., and Pavlides, S.: Palaeomagnetic analysis on pottery as indicator for the pyroclastic flows deposit temperature: New data and statistical interpretation from the Minoan eruption of Santorini, Greece, Geophys. J. Int., 203, 33–47, https://doi.org/10.1093/gji/ggv267, 2015.

Thouret, J. C., Arapa, E., Charbonnier, S., Guerrero, A., Kelfoun, K., Cordoba, G., Rodriguez, D., and Santoni, O.: Modeling tephra fall and sediment-water flows to assess their impact on a vulnerable building stock in the City of Arequipa, Peru, Front. Earth Sci., 10, 865989, https://doi.org/10.3389/feart.2022.865989, 2022.

Toyos, G., Gunasekera, R., Zanchetta, G., Oppenheimer, C., Sulpizio, R., Favalli, M., and Pareschi, M. T.: GIS-assisted modelling for debris flow hazard assessment based on the events of May 1998 in the area of Sarno, Southern Italy: II. Velocity and dynamic pressure, Earth Surf. Proc. Land., 33, 1693–1708, https://doi.org/10.1002/esp.1472, 2008.

Vallance, J. W. and Iverson, R.: Lahars and their deposits, in: Encyclopedia of Volcanoes, edited by: Sigurdsson, H., Houghton, B. F., McNutt, S. R., Rymer, H., and Stix, J., Academic Press, London, 649–664, https://doi.org/10.1016/B978-0-12-385938-9.00037-7, 2015.

Vallance, J. W. and Scott, K. M.: The Osceola Mudflow from Mount Rainier: Sedimentology and hazard implications of a huge clay-rich debris flow, Geol. Soc. Am. Bull., 109, 143–163, 1997.

Vitale, S. and Ciarcia, S.: Tectono-stratigraphic setting of the Campania region (southern Italy), J. Maps, 14, 9–21, https://doi.org/10.1080/17445647.2018.1424655, 2018.

Voight, B.: The 1985 Nevado del Ruiz volcano catastrophe: anatomy and retrospection, J. Volcanol. Geoth. Res., 42, 151–188, 1990.

Waitt Jr., R. B., Pierson, T. C., MacLeod, N. S., Janda, R. J., Voight, B., and Holcomb, R. T.: Eruption-triggered avalanche, flood, and lahar at Mount St. Helens – Effects of winter snowpack, Science, 221, 1394–1397, https://doi.org/10.1126/science.221.4618.1394, 1983.

Walsh, B., Coviello, V., Capra, L., Procter, J., and Marquez-Ramirez, V.: Insights into the internal dynamics of natural lahars from analysis of 3-component broadband seismic signals at Volcan de Colima, Mexico, Front. Earth Sci., 8, 542116, https://doi.org/10.3389/feart.2020.542116, 2020.

Whipple, K. X., Hancock, G. S., and Anderson, R. S.: River incision into bedrock: Mechanics and relative efficacy of plucking, abrasion, and cavitation, Geol. Soc. Am. Bull., 112, 490–503, https://doi.org/10.1130/0016-7606(2000)112<490:RIIBMA>2.0.CO;2, 2000.

White, S., García-Ruiz, J. M., Martí-Bono, C., Valero, B., Errea, M. P., and Gómez-Villar, A.: The 1996 Biescas campsite disaster in the Central Spanish Pyrenees and its spatial and temporal context, Hydrol. Process., 11, 1797–1812, https://doi.org/10.1002/(SICI)1099-1085(199711)11:14<1797::AID-HYP605>3.0.CO;2-7, 1997.

Zanchetta, G., Sulpizio, R., and Di Vito, M. A.: The role of volcanic activity and climate in alluvial fan growth at volcanic areas: an example from southern Campania (Italy), Sediment. Geol., 168, 249–280, https://doi.org/10.1016/j.sedgeo.2004.04.001, 2004a.

Zanchetta, G., Sulpizio, R., Pareschi, M. T., Leoni, F. M., and Santacroce, R.: Characteristics of May 5–6, 1998 volcaniclastic debris flows in the Sarno area (Campania, southern Italy): relationships to structural damage and hazard zonation, J. Volcanol. Geoth. Res., 133, 377–393, https://doi.org/10.1016/S0377-0273(03)00409-8, 2004b.

Zanella, E., Gurioli, L., Pareschi, M. T., and Lanza, R.: Influences of urban fabric on pyroclastic density currents at Pompeii (Italy): 2. Temperature of the deposits and hazard implications, J. Geophys. Res., 112, B05214, https://doi.org/10.1029/2006JB004775, 2007.

Zanella, E., Gurioli, L., Lanza, R., Sulpizio, R., and Bontempi, M.: Deposition temperature of the AD 472 Pollena pyroclastic density current deposits, Somma-Vesuvius, Italy, B. Volcanol., 70, 1237–1248, https://doi.org/10.1007/s00445-008-0199-9, 2008.

Zanella, E., Sulpizio, R., Gurioli, L., and Lanza, R.: Temperatures of the pyroclastic density currents deposits emplaced in the last 22 kyr at Somma-Vesuvius (Italy), Geological Society, London, Special Publication, 396, 13–33, https://doi.org/10.1144/SP396.4, 2015.

Zaragoza, G., Caballero-Garcia, L., Capra, L., and Nieto-Torres, A.: Lahares secundarios en el volcan Popocatepetl: El lahar Nexpayantla del 4 de febrero, 2010, Rev. Mex. Cienc. Geol., 37, 121–134, https://doi.org/10.22201/cgeo.20072902e.2020.2.1565, 2020.

Zuccaro, G. and De Gregorio, D.: Time and space dependency in impact damage evaluation of a sub-Plinian eruption at Mount Vesuvius, Nat. Hazards, 68, 1399–1423, https://doi.org/10.1007/s11069-013-0571-8, 2013.